THANKS

TO

ALMIGHTY ALLAH

PROCESSING AND CHARACTERIZATION OF CALCINED AND SINTERED DONOR DOPED BARIUM TITANATE

ANINDA NAFIS AHMED

STUDENT NUMBER 0411112018

DEPARTMENT OF MATERIALS AND METALLURGICAL ENGINEERING

BANGLADESH UNIVERSITY OF ENGINEERING AND TECHNOLOGY

DHAKA, BANGLADESH

NOVEMBER, 2014

PROCESSING AND CHARACTERIZATION OF CALCINED AND SINTERED DONOR DOPED BARIUM TITANATE

BY

ANINDA NAFIS AHMED

STUDENT NUMBER 0411112018

THIS THESIS PAPER IS SUBMITTED TO THE DEPARTMENT OF

MATERIALS AND METALLURGICAL ENGINEERING AS PARTIAL

FULFILLMENT OF THE REQUIREMENTS

FOR

THE DEGREE OF MASTER OF SCIENCE IN MATERIALS AND METALLURGICAL ENGINEERING

DEPARTMENT OF MATERIALS AND METALLURGICAL ENGINEERING

BANGLADESH UNIVERSITY OF ENGINEERING AND TECHNOLOGY

DHAKA, BANGLADESH

CANDIDATES' DECLARATION

IT IS DECLARED HEREBY THAT THIS THESIS PAPER OR ANY PART OF IT HAS NOT BEEN SUBMITTED TO ANYWHERE ELSE FOR THE AWARD OF ANY DEGREE

.....

Aninda Nafis Ahmed

.....

Supervisor

Dr. Hossain Mohammad Mamun Al Rashed

The thesis titled **"Processing and Characterization of Calcined and Sintered Donor Doped Barium Titanate**" Submitted by Aninda Nafis Ahmed, Student Number: 0411112018, Session: April 2011 has been accepted as satisfactory in partial fulfillment of the requirements for the degree of Master of Science in Materials and Metallurgical Engineering on 15 November 2014

Board of Examiners

. . . . . .

Chairperson
Dr. Hossain Mohammad Mamun Al Rashed
Assistant Professor, MME, BUET.

. . . . . .

Member (Ex-Officio)
Dr. Ahmed Sharif
Professor and Head, MME, BUET.

. . . . . .

Member
Dr. Kazi Mohammad Shorowordi
Assistant Professor, MME, BUET.

. . . . . .

Member (External)
Dr. A. K. M. Abdul Hakim
Director (Retd.), Planning and Development Division
Bangladesh Atomic Energy Commission, Dhaka.

Dedicated to

My Family

ACKNOWLEDGEMENT

I would like to express my deep and sincere gratitude to my supervisor and respected mentor Dr. H. M. M. A. Rashed for his patience, motivation, enthusiasm and guidance, in spite of his busy schedule. His understanding, personal guidance and support has provided me good basis for my work.

I also would like to convey my heartiest regards to my respected teacher Professor Dr. Md. Fakhrul Islam for giving me guidance on the technical part of my research. Being a very busy person, he spared me his valuable time and pointed my work towards right directions. I am very much thankful to him for his priceless advices.

Despite various limitations, the Department of Materials and Metallurgical Engineering and the Department of Glass and Ceramic Engineering have provided me continuous access to some of the finest and advanced equipments through this thesis for which it has been possible to perform this research. Along with my experiments, all these facilities have also helped me out in enriching my technical and operational experiences. Furthermore, Department of Materials and Metallurgical Engineering has provided me sufficient fund to support my thesis work. That is why, I would like my express my utmost gratitude to the Department of Materials and Metallurgical Engineering and to the Department of Glass and Ceramic Engineering.

I pay my gratitude to Dr. Abdul Gafur and Md. Rakibul Qadir of BCSIR for supporting with XRD, Md. Aminur Rahman and Mst. Shanjida Sultana of BCSIR for supporting in particle size analysis. These supports have been very important in my research. I owe special thanks to Md. Muktadir Billah, lecturer MME and Arman Hossain, Lecturer GCE for their support.

I also thank Mr. Yousuf Khan, Mr. Rana for support in electron microscopy, Mr Maksud for helping in handling different equipment, Mr. Ahmadullah and Mr. Shahjalal for their support in the laboratory.

Finally, I express thanks to all my teachers, seniors and friends who have supported directly and indirectly to complete my work by information and inspiration.

ABSTRACT

Formation and development of microstructure of Nb doped $BaTiO_3$ was investigated through the mixed oxides route via the process of calcination based on the formula $BaTi_{1-x}Nb_xO_3$ where x=0.004, 0.008, 0.016. Calcination temperature of 1300°C was found to be appropriate by XRD data regarding the formation of perovskite structures when Nb doped $BaTiO_3$ patterns were compared with standard $BaTiO_3$ pattern. From the XRD patterns, peaks corresponding to (002) and (200) planes suggested that increasing Nb doping level reduced the tetragonality of barium titanate as found by plotting c/a ratio against doping level. Non-uniform distribution of Nb was observed when the calcined product showed different Nb concentrations at different regions, found in Energy-dispersive X-ray spectroscopy study. Particle size analysis data indicated bimodal distributions of calcined product for all three doping levels being calcined from $BaCO_3$, TiO_2 and Nb_2O_5 where starting raw materials had different sizes and distributions. Moreover, submicron-size particles were produced in each case of the calcined product for all three doping levels. However, with the addition of Nb, particle size was reduced gradually probably due to the pinning effect of Nb on particle size.

Above 90% of theoretical density was achieved for samples having different doping levels sintered around 1450°C. Consistency in the grain growth behavior was observed when microstructures were studied by scanning electron microscope.

Maximum dielectric constant at room temperature was recorded above 10,000 for the samples containing 0.4 mol% Nb being sintered at 1450°C. Shifting of Curie temperature occurred towards lower temperature than that of pure $BaTiO_3$ due to the addition of Nb. Nb addition has resulted low dielectric constant values beyond 0.8 mol% Nb doping due to loosing of tetragonality and stabilizing cubic or pseudocubic structure which are detrimental for polarization of dielectric materials.

In order to generate the significance of variables, a statistical modeling by ANOVA (analysis of variance) was performed on different sintering parameters and frequencies for some particular set of data. It was evident that sintering temperature had stronger effect than doping level of Nb in determining the density of niobium doped $BaTiO_3$ whereas Nb concentration had stronger effect in determining the grain size over sintering temperature. Furthermore, profound effect of frequencies in determining dielectric constant of $BaTiO_3$ was observed when it was compared with holding time during sintering, as applied frequency strongly controlled the polarization of material.

Table of Contents

List of Figures

List of Tables

Chapter 2

Chapter 3

Chapter 4

List of Abbreviations

ANOVA: Analysis of Variance

$BaTiO_3$: Barium Titanate

$BaCO_3$: Barium Carbonate

EDX: Energy Dispersive X-Ray

FESEM: Field Emission Scanning Electron Microscopy

k: Dielectric Constant

MLCC: Multi Layer Ceramic Capacitors

Nb_2O_5: Niobium (V) Oxide

SEM: Scanning Electron Microscopy

TiO_2: Titanium dioxide

Tc or θc: Curie temperature

XRD: X-ray Diffraction

XRF: X-ray Fluorescence

Chapter 1

Introduction

Barium titanate ($BaTiO_3$) is one of the pioneer materials in the field of dielectrics. Due its crystal structure, barium titanate possesses distinctive structural characteristics. Remarkable electronic properties can be observed from $BaTiO_3$ [1]. Versatile applications of $BaTiO_3$ in the field of dielectric ceramics have been revealed to the scientific world such as capacitors, transducers, thermistors etc. As a consequence, $BaTiO_3$ for 60 years, has been one of the major candidates in the field of electronic applications.

Thermal stability of structure, electronic response, chemical and physical stability are the properties of most interest as $BaTiO_3$ exhibits ferroelectric properties at and above room temperatures. Different applications have been observed for polycrystalline $BaTiO_3$ as ferroelectric material. For example, MLCCs or multilayer ceramics capacitors having high dielectric constant and low loss. $BaTiO_3$ has piezoelectric properties and can be used for microphones and other transducers. Polycrystalline $BaTiO_3$ also has positive temperature coefficient, which is appropriate for thermistor. Furthermore, it is also used as sensors and energy storing devices. Use of $BaTiO_3$ in transducers, actuators and ferroelectric random access memories (FRAM) has also been reported [2].

As the era of miniaturization is going on, the high dielectric constant values in small volume is always desired which will result large capacitance per unit volume. In present days, nearly one micron of dielectric thickness and 1000 layers of dielectrics in MLCCs are being manufactured [3].

Dielectric properties of barium titanate can be engineered not only by controlling processing parameters but also by doping with metallic ions that can replace atoms at different positions of the lattice. For example, Ba^{2+} can be replaced by Pb^{2+}, Sr^{2+} ions; Ti^{4+}can be replaced by Nb^{5+}, Zr^{4+}, Hf^{4+} ions. Doping and processing parameters directly affect the structure of barium titanate which influences the ferroelectric behavior. Doping may cause diffusion of donor ion into $BaTiO_3$ grain causing Ti segregation on grain boundaries restricting grain growth [4]. This can bring modifications in microstructure and produce variations in properties. There are several factors which individually or combinedly, influence the behavior of barium titanate based dielectrics. Grain size and grain boundaries , size and distribution of impurities, stress imposed by

surrounding grains, presence of secondary phases, initial raw material conditions and process variables are the most important ones. Fine grain structure with minimum porosity and high density without harmful secondary phases are always required for better dielectric properties.

The present work includes the formation and characterization of donor doped barium titanate based ceramics. Nb was used as donor in this work, which has 5+ charge in ion form. Nb doped $BaTiO_3$ was prepared by mixed oxide route through the process of calcination by calcining $BaCO_3$, TiO_2 and Nb_2O_5 at 1300°C. 0.4, 0.8 and 1.6 mol% Nb was doped into $BaTiO_3$. This study covers up the particle size analysis, electron micrographs study before and after calcination. XRD analysis was preformed after calcination in order to confirm the pervoskite $BaTiO_3$ formation. Identification of secondary phases was also done in this regard. Doping effect on tetragonality was studied from the twin peaks of XRD patterns. EDX was performed in understanding the diffusion of Nb in $BaTiO_3$ after calcination and XRF analysis was also done to know the amount of recovered material in comparison to the raw materials after sintering around 1350-1550°C. Sintering parameters were optimized by trial and error method for 0.4 mol% Nb, measuring all the required properties like density, grain size and dielectric properties. Later, final experiments were carried out for all three doping level around the optimized parameters. ANOVA modeling was done on different sets of experiments and certain significant variables were identified for different conditions.

This work will provide sufficient information in producing $BaTiO_3$, doped with Nb, by calcination. Moreover, particle size distribution, microstructural features and EDX study, before and after calcination, will reveal important information about Nb diffusion and grain size after final sintering. Important variables identified from ANOVA modeling can be tuned further in improving properties. Furthermore, effects of Nb addition on density, grain size, and dielectric properties will be revealed.

The research work is arranged in several chapters. Chapter two discusses about the background of dielectrics, polarization mechanisms and how dielectrics work. Then the chapter focuses on $BaTiO_3$, its atomic structure, how does it produces polarization and what are the techniques in producing and manipulating its properties. Finally, recent works on $BaTiO_3$, areas of the present research and scope future research have been described.

Chapter three explains the materials, experimental techniques that have been followed so far in milling, calcining, pressing, and sintering the samples. Moreover, information about characterization techniques is mentioned, which were followed in measuring density, grain size, dielectric properties and statistical modeling.

Finally, chapter four describes the results and relevant discussions, which have been obtained so far. Particle size analysis, XRD for all three doping levels are included in this chapter. Additionally, effects of different sintering parameters on different properties have been illustrated from which a set of optimum sintering parameters was developed. Overall, effects of doping on microstructures, density, grain size and dielectric properties have been discussed extensively in this chapter. Moreover, an attempt to correlate these properties has been made.

At the end of chapter four, the major outcomes of this work have been listed, which states the findings of this research.

Chapter 2

Literature Review

2.1 Introduction

Conducting materials are good conductor of electricity. They permit the flow of charges in one or different directions. Generally, metallic materials are good conductors of electricity as they have sea of free electrons generated from metallic bonds. On the other hand, in insulators, electrical charges do not flow freely and restrict the flow of charge under an applied electric field. Typically there is a group of materials specially ceramics materials that show insulating properties. Therefore, dipole structure can be prepared by combining conductors and insulators. Two conductor plates mainly metallic and an insulating ceramic material sandwiched between them can produce such structure. This type of arrangement can show charge storing ability, rather than passing through the conductors via the insulator under an applied electric field. The charge storing capacity of the insulating material is called dielectric properties and the material itself is called dielectric.

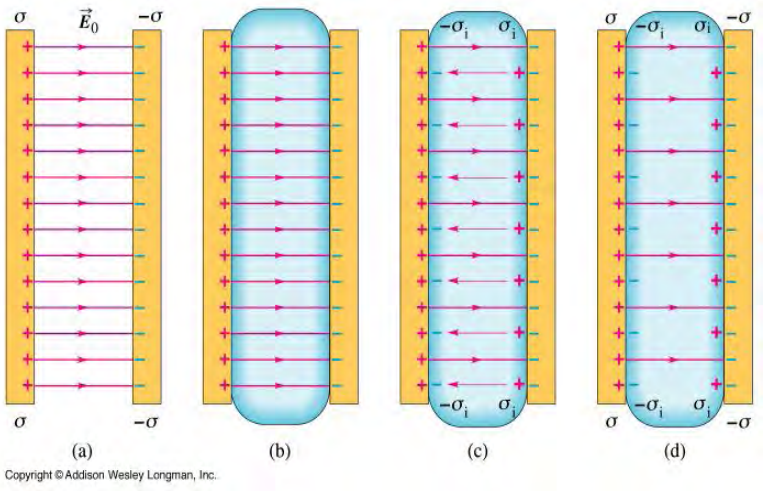

Figure 2.1 (a) Electric Field of Magnitude E_o between Two Charged Plates,(b) Dielectric being Placed in between (c) The Surface Charges Induced and Their Field (Thinner Lines).(d) Resultant Field of Magnitude Eo/K when a Dielectric is between Charged Plates [5]

Dielectrics in capacitors keep the conductor plate away from each other and ensure small distance between conductor plate resulting high capacitance. It also reduces electric field strength and increases effective capacitance. For this reason, at lower voltage, same amount of charge can be stored. Furthermore, it reduces the possibility of

shorting during operation at high temperature, a phenomenon termed as dielectric breakdown.

2.2 Dielectrics

The main use of dielectric materials is in the field of capacitors and properties associated with dielectrics are dielectric constant, dielectric loss factor and dielectric strength. As a result, the concept of capacitance must be cleared.

If a simple parallel plate capacitor is considered with metal plate having area A each, separated by a distance of d and the medium between the plate is vacuum, then under an applied voltage of V across the plates, one of the plates will gain a net charge of +q and the other will gain -q. The charge will be directly proportional to the applied voltage according to the relations as follows:

$$q=CV$$

$$\text{or} \quad C=\frac{q}{V} \quad \text{---------- (1)}$$

Where, C is the proportionality constant called capacitance of the capacitor having the unit in S.I. format, coulombs per volt C/V or Farad (F) [5]. It is the ability of charge storing capacity. The higher the capacitance, the higher the charge storing capacity. The capacitance of a parallel plate capacitor having a vacuum between the plates is termed as follows:

$$C_0 = \frac{A}{d} \in_o \quad \text{---------- (2)}$$

Where, A = area of the plates, D = distance between the plates, $\in 0$ =permittivity of vacuum, constant having a value of 8.85×10^{-12} F/m.

Instead of a vacuum, if a dielectric material can be placed between the plates, then the capacitor's capacitance will be changed by a factor of k, which is called dielectric constant of the material. In that case the capacitance will be

$$C = \frac{A}{d} \in_0 k$$

$$\text{or} \quad C = \frac{A}{d} \in \quad \text{----------(3)}$$

Where, $\in$ = permittivity of the dielectric medium greater than $\in_0$, the factor k is called relative permittivity or dielectric constant of the dielectric material which is equal to the ratio of the permittivity of the dielectric medium to that of vacuum (Equation 4).

$$k = \in/\in_0 \quad \text{---------- (4)}$$

The schematic of this theory is shown in Figure 2.2

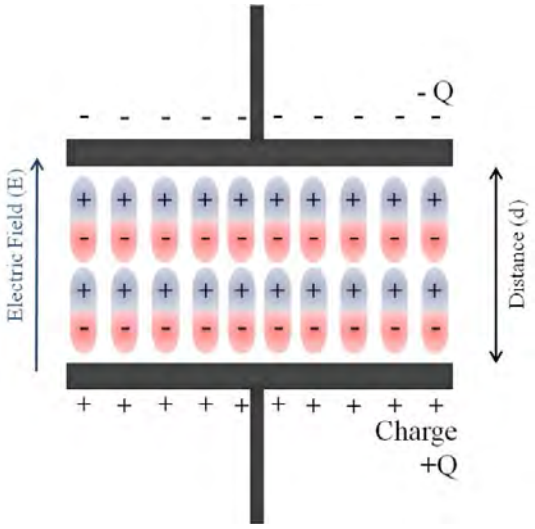

Figure 2.2 Capacitor Schematic with Dielectric [6]

The k value of the dielectric is greater than unity, indicating the higher capacity of charge storing of dielectric materials than the vacuum. The resultant electric field is somewhat lower than the applied field, as the charges induced on surface produces an opposite electric field to the applied field, which in turn, reduces the original field by cancelling each other.

2.3 Polarization

When the atoms or molecules of a dielectric material are placed in an external electric field, the nuclei are pushed with the field resulting in an increased positive charge on one side while the electron clouds are pulled against it resulting in an increased negative charge on the other side. This process is known as polarization and a dielectric material in such a state is said to be polarized [7]. Stretching and rotation are two of the major methods of polarization of dielectric materials.

From Equations 1 & 2 the surface charge Q, in vacuum,

$$\sigma vac = \left[\frac{Q}{A}\right] vac = \varepsilon o \left(\frac{V}{d}\right) = \varepsilon oE \quad \text{..... (5)}$$

Where, E= Applied electric field across the plates of the capacitor, V/m. Similarly, Equation 1 & 3 point to the surface charge on the metal plates with dielectrics

$$\left[\frac{Q}{A}\right] Die = \varepsilon ok \left(\frac{V}{d}\right) = \sigma vac + \sigma pol \quad \text{..... (6)}$$

Where, σpol = excess charge per unit surface area present on the dielectric surface. This numerically has the same dimension as the polarization, P of the dielectric material.

$$\sigma pol = P \text{ ..... (7)}$$

The total charge can be divided to free charge Q/K that sets up the electric field & voltage toward the outside; the other portion being the bound charge, is neutralized by polarization of the dielectric. Schematically, it can be represented that the total electric flux density D is the sum of the electric field E & the dipole charge P:

$$D = \varepsilon oE + P = \varepsilon' E \text{ ..... (8)}$$

Polarization P is the surface charge density of the bound charge, equal to dipole moment per unit volume of material.

$$P = N\bar{\mu} \text{ ..... (9)}$$

In other words, the total charge on the capacitor D is the sum of the charge that is present in vacuum & an extra charge that results from the polarization of the dielectric material P. Thus polarization can equivalently designate either the bound charge density or the dipole moment per unit volume. From equation 8-

$$P = \varepsilon' E - \varepsilon oE = \varepsilon o(k-1)E = \chi die\, \varepsilon oE \text{ ..... (10)}$$

Where, χdie = Dielectric susceptibility of the material

$$\chi die = k - 1 = \left(\frac{p}{\varepsilon oE}\right) \text{ ..... (11)}$$

The susceptibility is the ratio of the bound charge density to the free charge density.

Considering from microscopic point of view, the charge carriers in dielectric materials cause to react with & affect the electromagnetic radiation. The relationship between applied field & the medium can be considered as resulting from the presence of elementary electric dipoles having an average dipole moment, $\bar{\mu}$. If the dipole moment is represented by two charges of the opposite polarity, +Q & -Q, separated by a distance δ & then $\bar{\mu}$ equals (Qδ).

$$\bar{\mu} = Q\delta \text{ ..... (12)}$$

With the above considerations, if the centre of electron charge moves by an amount δ , Then the total volume occupied by these electrons would be (Aδ). If the number of molecules per unit volume by N then the total charges appearing in that volume (Aδ) is (Aδ NQ).

Over the range of optical frequencies, the source of this dielectric polarization is the shift of the electric cloud around the atomic nucleus. The average dipole moment is proportional to the local electric field strength (E) that acts on the particle, the proportionality constant (α) being called the polarizability.

$$\overline{\mu} = \alpha E \quad \text{..... (13)}$$

Regarding to the statement & Equation 9, it can be concluded that-

$$P = N \alpha E \quad \text{..... (14)}$$

From Equation 14, an idea of polarization per unit volume of a dielectric with the presence of an electric filed can be obtained.

2.4 Polarization Mechanisms

Electric dipole formation is called polarization. There are several mechanisms that contribute to the formation of dipoles. Electronic polarization, orientation or dipolar polarization, space charge polarization and, atomic or ionic polarization are the four major types of polarization mechanisms [8].

2.4.1 Electronic Polarization

This type of polarization occurs in all dielectric materials where the electrons around the nucleus shift slightly toward the positive electrode and the nucleus shifts slightly towards negative electrode. With the removal of electric field the polarization disappears as the electrons and nucleus return to their original distribution. The shift of charge is small compared to the other mechanisms of polarization. That is why, electronic polarization results small amount of dipole formation Figure 2.3 [8].

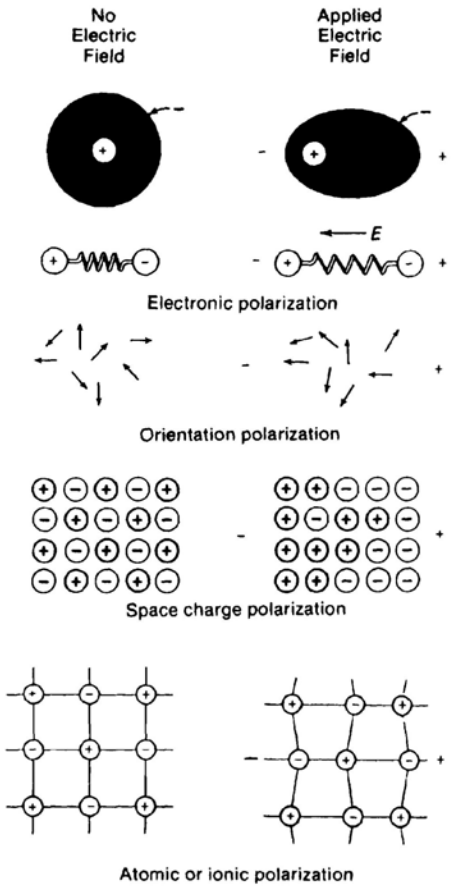

Figure 2.3 Mechanisms of Polarization [8]

2.4.2 Orientation or Dipolar Polarization

Non symmetric molecules containing permanent electrical dipole cause this type of polarization (Figure 2.3). For example, in water molecules (H_2O), hydrogen and oxygen are bound to each other by covalent bond which is directional. The hydrogen side of the molecule has net positive charge and oxygen side has net negative charge. So under an applied electric field, the positive side will shift towards negative electrode and vice versa creating dipoles. This type of polarization has much stronger effects than the electronic polarization. Larger displacement is possible in orientation polarization than electronic, where the displacement of electron and nucleus is very low.

2.4.3 Space Charge Polarization

Space charge polarization is caused by random charges generated from cosmic radiation and thermal deterioration or by charges trapped during fabrication process. Charges may develop in the interfaces like grain or phase boundaries as a result of impurities. Movement of charges occurs when material is placed under an electric field. The mechanism of this type of polarization is not well resolved but they are of practical interest as ceramics materials possess impurities.

2.4.4 Atomic or Ionic Polarization

It is the displacement of atom or ion which occurs with the application of electric field within a crystal structure. Larger effect in displacement thus polarization can be observed by this mechanism, depending on crystal structure. Solid solution and other factors can play an important role in this regard. Pyroelectricity, piezoelectricity and ferroelectricity are highly discussed on the basis of this polarization.

2.5 Polarization as a Function of Frequency

The dipoles in dielectric tend to align with field of application when a field is applied across a dielectric material. This requires a finite amount of time which is separated for different polarization mechanisms. At the relaxation frequency, the dipoles will only be able to reorient themselves in time with the applied field. At this point, the dielectric is in the losing side and loss of energy occurs in the form of heat. The loss maximizes when the relaxation frequency of a particular mechanism matches with the frequency of external or applied field. If the applied frequency is greater than the relaxation frequency, then the dipoles become unable to keep up with the field and the mechanism's effectiveness freezes. The frequency dependency of polarization mechanism is shown in Figure 2.4.

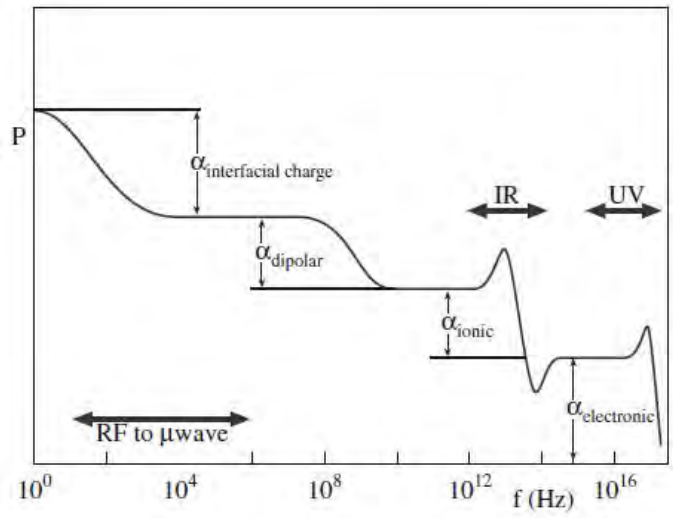

Figure 2.4 Frequency Dependence of Polarization Mechanisms [7]

2.6 Dielectric Constant

The charge storing capacity of a dielectric material can be indicated by relative dielectric constant k'. This also called relative permittivity. If an electric field is applied across a parallel plate capacitor, charge will be accumulated in the capacitor. For both vacuum and dielectric material the schematic is given in Figure 2.5.

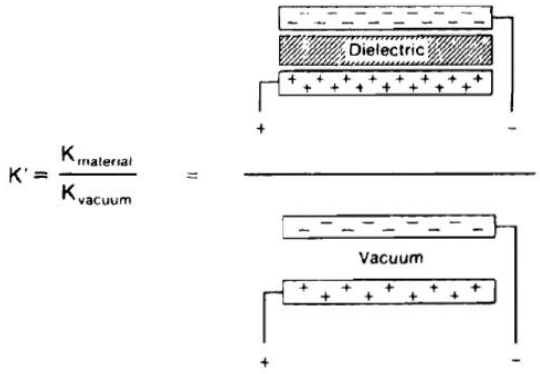

Figure 2.5 Illustration of Relative Permittivity or Dielectric Constant [7]

Both materials between the parallel plates will be polarized and the relative dielectric constant will be the ratio of charge storing capacity of the dielectric material to that of vacuum. Dielectric constant is a function of temperature and frequency. However, different polarization mechanism has different behavior with temperature. Electronic polarization has minimum effect of temperature. Molecular orientation polarization is inversely affected by thermal agitation; as a result, dielectric constant will go down with increasing temperature. Atomic or ionic polarization increases with temperature as higher temperature increases the charge mobility or ion movement. The dielectric constant is also a strong function of applied frequency and this has been illustrated in Section 2.5, where polarization is explained as a function of frequency.

2.7 Dielectric Loss

Dielectric material theoretically does not allow the flow of charges through the electrode placed either side of the material by creating small displacement of charge. If an alternating electric field is applied across a capacitor, and current leads voltage by an angle of 90°, no power would be absorbed by the dielectric and the capacitor would have zero loss. However, in reality, the material suffers some loss, and the current lags voltage slightly than the ideal case. The angle is defined as δ and the amount is tanδ, which is the amount of lag. tanδ is also known as loss tangent and can be defined as the ratio of k"/k', where k' is the relative dielectric constant and k" is the relative loss factor. Dielectric loss may result from three mechanisms: ion migration; ion vibration and deformation, and electronic polarization. Ion migration which is strongly affected by temperature and frequency, is one of the important mechanisms for ceramics materials. Loss from ion migration increases at lower applied frequencies and higher temperatures [8].

2.8 Dielectric Strength

It is the materials ability to withstand under an applied electric field without leaking current through the capacitors. The unit is volt per unit thickness of the dielectric material. Volt per centimeter is often used as unit of dielectric strength of materials [8]. This defines the voltage per unit length at which failure occurs. This is the maximum electric field that a dielectric material can sustain without an electrical breakdown.

At low field strength, a certain level of dc conductivity generates with the mobility of charges arising from electronic and ionic imperfections or defects. By increasing the field strength, this dc conduction increases. When a large value of potential is reached, field emission from the electrodes causes flow of electron and produces a surge of current that produces breakdown channels, jagged holes or metal dendrites bridging the dielectric. This results in failure of the dielectric. Dielectric breakdown of material may take place in two different ways; electronic breakdown and thermal breakdown.

2.8.1 Electronic Breakdown

Electronic breakdown is also referred as intrinsic dielectric strength, where the voltage gradient, which is localized, reaches a critical value. In this case, the electrons in conduction band are accelerated by the field that permits flowing of additional electrons coming out of collisions and ionizing constituent ions [2]. This stimulation continues until an avalanche of electron is created resulting breakdown and sample rupture. Below room temperature, the electronic breakdown increases with temperature for crystalline materials. Lattice vibrations and electron scattering increase with increasing temperature, which in turn, produce the avalanche of electron. This leads to the failure of dielectric. Glassy material's breakdown is independent of temperature at low temperature.

2.8.2 Thermal Breakdown

This type of breakdown is caused by local overheating generated from the process of electrical conduction. The local conduction increases to such a point that allows flow of current causing puncture, melting and so on. Thermal breakdown increases with increasing temperature and applied voltage input time.

This type of breakdown is attributed to the electrical stress of sufficient time so that local heating can take place. Sufficient temperature has to be reached to increase the electrical conductivity. Faster heat generation inside the dielectric, than dissipation to the surroundings, increase conductivity and dielectric loss [2]. Thermal breakdown as already mentioned causes channeling of currents, local instability and high passage current with fusion and vaporization. These in turn, puncture the dielectric.

2.9 Class of Electro-ceramics Materials

2.9.1 Piezoelectric Ceramics

When an electric field is applied to a material, a small change in dimension occurs in the material. If the resultant strain is proportional to the square of the field, then it is termed as electrostricitve effect. Contrarily, some materials show reverse effect developing electric polarization when it is strained by applying stress. These are called piezoelectric materials and the property is termed as piezoelectricity. Piezoelectricity can be explained by the crystals having nonsymmetrical unit cell where displacement of ions can occur. Being compressed, ions of each unit cell cause electric polarization by displacing themselves. Because of the repetitive nature of crystalline material these effects accumulate and a resultant potential difference grows between certain faces of the crystal. Piezoelectric effect has two aspects; direct polarization effect and indirect polarization effect. When a piezoelectric material is subjected to a compression or physical distortion, it gains electric charge which is termed as direct polarization effect. On the other hand, when the material is subjected under an applied electrical field, mechanical stress is found on the material which is known as indirect polarization effect. Direct and indirect polarization effects have been illustrated in Figure 2.6.

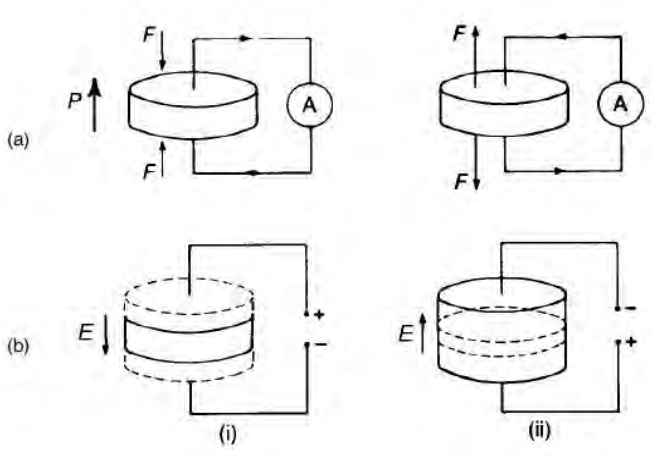

Figure 2.6 (a) The direct and (b) The Indirect Piezoelectric Effects: (i) Contraction; (ii) Expansion. Dashed Lines Indicating the Original Dimensions [2]

There are 32 crystal systems, among them twenty are piezoelectric. Again twenty one among these 32 systems are non-centrosymmetric; not having a centre of symmetry, and twenty of them show direct piezoelectricity. Ten of them are polar having dipole in the unit cell which polarizes spontaneously and certainly shows piezoelectricity. If the dipole can be reversed by applying an electric field then it is called ferroelectricity. But the piezoelectric material does not have charge storing capacity with the removal of force, whereas the dielectric material has it with the removal of external electric field.

2.9.2 Pyroelectric Materials

Pyroelectric material has spontaneous polarization effect which is a function of temperature. More specifically, it is the ability of material to generate electric potential when it is heated or cooled. The dipole moment varies when the crystal is heated or cooled as they get expanded or contracted. This effect occurs to the crystal which lacks center of symmetry and also has polar direction. Only ten of the thirty two crystal system can fulfill this type of requirement. $LiTaO_3$, $BaTiO_3$ are the examples of this pyroelectric crystal. When crystal is heated to a constant temperature this polarization does not comes into play as it is compensated by the conduction free charge carrier that reaches the surface of the crystal through it and also from the surroundings. But when the crystal's temperature is raised or lowered, the permanent polarization changes, which is originally possessed by the pyroelectric crystal, and polarization comes into play. Only ten of the thirty two crystal systems are pyroelectric. Because they are polar in structure and polarity is fully dependent on the crystal structure.

Large electric field can be developed across a pyroelectric material when it is subjected to a small change in temperature. Pyroelectric coefficient p can be defined as the change in D (charge density) due to a change in T (temperature) where, p has unit in $Cm^{-2}K^{-1}$ [7]

$$p = \partial D / \partial T$$

2.9.3 Ferroelectric Ceramics

Ferroelectric materials show dipole moment in absence of an external electrical field. The dipole moment direction may swing depending on the alternating external applied electric field. The properties of polarization reversal, remnant polarization cannot be detected based on the structure of the material. However, it has to be determined experimentally. Not only ceramics but also polymeric materials also show ferroelectricity, for example PVDF or polyvinylidene fluoride.

Ferroelectric material follows a path of hysteresis loop with the application of an external electric field in case of spontaneous polarization. For a perfectly cubic crystal, ferroelectricity is nearly impossible. Ferroelectric materials shows ferroelectricity below a certain critical temperature which is known as Curie temperature T_c (θ_c) and above this temperature material becomes paraelectric. Crystal structure is very important in determining the ferroelectric behavior. A non centric crystal is must, containing alternate atom position, to allow reversal and retention of polarization after the reversal or removal of field respectively. In case of barium titanate the crystal structure is cubic above 120°C, thus not showing ferroelectricity. In this case, the Ti^{4+} is located in the octahedral site of the lattice and can move into six possible sites causing polarization with the application of an electric field but with the withdrawal of the field titanium will get back to its original position resulting no net

polarization. Hence, no ferroelectric behavior is observed. However, below 120°C the structure becomes tetragonal, which forces the titanium ion to shift in an off-centered position resulting spontaneous polarization thus showing ferroelectricity.

Ferroelectric material also shows piezoelectricity and pyroelectricity but the reverse does not hold true. Moreover, ferroelectricity is a function of temperature. Higher temperature disturbs the alignment of electric dipoles by thermal vibration. As a result, with temperature ferroelectric property deteriorates. The alignment is lost and Curie-Weiss law holds. The relative permittivity shows characteristic peaks at T_{cw} showing in Figure 2.7 and starts to fall beyond T_{cw} which is the Curie-Weiss law: $\varepsilon_r - 1 = \chi = C/(T-T_{cw})$, Where, ε_r is relative permittivity, χ is electrical susceptibility, T is temperature and C is curie constant.

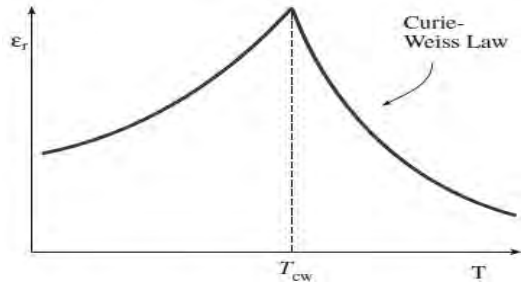

Figure 2.7 Relative Permittivity of Ferroelectric Material for as a Function of Temperature [7]

2.9.3.1 Ferroelectric Domains

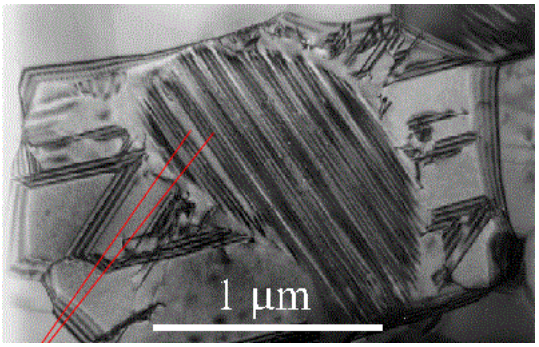

Figure 2.8 Ferroelectric Domain [9]

As the material develops its charge, a domain structure is developed to attain the minimum free energy for the crystal. Ferroelectric domains are the region in the crystal of local dipole alignment. These are associated with net dipole moment and polarization. Domains are separated by domain wall from each other. Domain walls are designated according to the angle between the domains. 90° or 180° boundaries are the most common ones.

With the applied external electric field, the domains grow and align themselves with the direction of the field at the expense of the less aligned ones. The domain structure can change with time through the process of aging. This may cause the deterioration of dielectric properties and device failure due to loss of insulation resistance.

Barium titanate tetragonal crystal may contain some dipoles in one part of the crystal directing towards a particular direction whereas, some dipoles in different directions commonly 90° or 180° away from the previous one. The regions where the dipoles are aligned in a common direction in the crystal are the domains.

Maximum of alignment of dipoles is desired during the application of an external electric field. Temperatures play an important role in this regard. For instance, maximum alignment under an applied electric field is observed for barium titanate by cooling it through 120°C, where transformation from cubic to tetragonal occurs. This is known as 'poling'. Maximum polarization can be found in this regards. It was found that, 180° domains are easy to remove than 90° domains because of the surface strain generated during cooling. Therefore, crystal fabrications can restrict domain motion. There may be many domains in a crystal separated by interfaces called domain walls.

2.9.3.2 Ferroelectric Hysteresis Loop

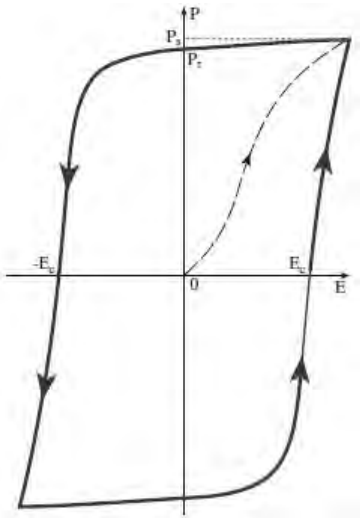

Figure 2.9 Response to an Applied Electric Field of Ferroelectric Material [7]

Ferroelectric material can retain dipoles or polarization in absence of the electrical filed. Moreover, reversal of polarization direction can also be observed with the application of appropriate electric field. Reverse field can reverse the polarization effects and produces a hysteresis loop. Such type of hysteresis loop is shown in Figure 2.9, indicating applied field as E and polarization as P. The domain in ferroelectric material is random before the application of electric field and net polarization is zero at zero field strength. When the field strength is low, the polarization is linear with the electric filed.

The slope of the curve gives the initial dielectric constant. At higher field strength the polarization increases rapidly as the ferroelectric domains switches and polarization direction changes in accordance with the applied field in domains by 90° or 180°. This can be occurred by the movement of domain boundaries along the crystal. At highest field strength the increase of polarization in specified field strength becomes less and saturation of polarization occurs. Here all domains get themselves aligned with the field. This is called saturation polarization P_s (Figure 2.9).

When the field is zero, polarization does not get to a value of zero but it has a definite value which is called remnant polarization indicated by P_r (Figure 2.9). This happens as some of the oriented domains become unable to get back to their original position or random state, without the additional opposite electric field. This additional energy is required to change the direction of the frozen domains. For getting the polarization zero, the required electric field is termed as coercive field E_c (Figure 2.9). At higher temperature the hysteresis loop becomes flatter and coercive force also becomes greater. Up to Curie temperature, coercive force decreases with the temperature. At Curie temperature, no hysteresis remains and a single value for the dielectric constant sustains. Both reversible and irreversible polarization is important in relation to the application. For memory device irreversible polarization is must and reversible polarization cannot be used. On the other hand, reversible polarization is important for dielectric materials that can be used in capacitors.

2.10 Science of Barium Titanate

This work concentrates on the processing and characterization of Nb doped barium titanate. Therefore, it is important to understand the science of barium titanate. The crystal structure possesses by barium titanate is called perovskite structure having the formula of ABO_3, where A and B are cations, and O is oxygen; definitely anion. The anions and cations form an array of FCC structure with an octahedron in the center of the cell. Ideal perovskite structure is simple cubic but mineral like $CaTiO_3$ is orthorhombic at room temperature and becomes cubic when heated above 900°C. Other ceramics those have perovskite structure are $BaTiO_3$, $SrTiO_3$, $KNbO_3$, etc. All of these can be written in the form of ABO_3 [7].

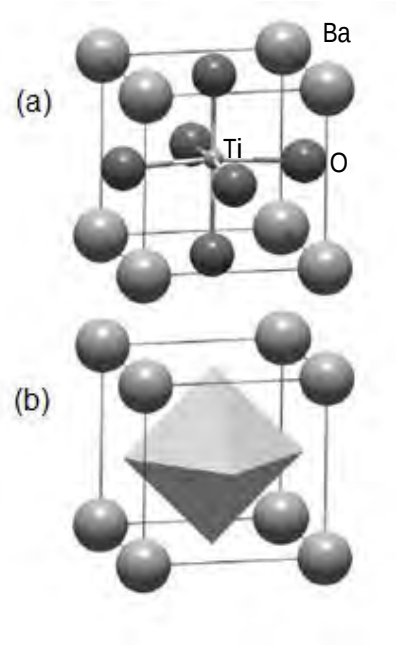

Figure 2.10 The Perovskite Crystal structure. The lattice is Simple Cubic with Several Cations Able to Occupy the Central Octahedron. (a) Atomic Model; (b) The Polyhedron. [7]

For ABO_3 type perovskite structure, O^{2-} and A^{2+} both have similar radii, where 'A' is the larger cation in comparison to 'B'. As a result, structure is not solely determined by oxygen. The larger cation and anion form a close packed arrangement with the smaller cation B^{4+} locating itself in the octahedral oxygen interstices. The octahedra then link together by sharing the corners showing in Figure 2.10(b). Barium titanate ($BaTiO_3$) is a prototype ferroelectric material having the ideal perovskite structure above 120°C and below this Curie temperature, the small cation Ti^{4+} shifts from the ideal symmetric position which is at the center of the octahedral holes. Electric dipole is created by such shifts, creating atomic or ionic polarization, changing the structural or unit cell dimension from cubic to tetragonal [7]. Perovskite structure is very important in terms of electrical properties. Ferroelectric properties, piezoelectric properties and high dielectric constant can be observed from such structures. Spontaneous polarization in absence of electricity is ferroelectricity (section 2.9.3) and electric field and mechanical deformation is linked with piezoelectricity (section 2.9.1).

$BaTiO_3$ is one of the most widely studied ceramic materials in the field of dielectrics. The invention of $BaTiO_3$ made it possible to take the value of dielectric constant (k) to two orders of magnitude than available previously. For this reason, $BaTiO_3$ has become the parent material for dielectric materials in capacitor mostly at doped condition. Several key factors have been identified from large number of researches that have been done on $BaTiO_3$. Simple crystal structure, durability and ferroelectric behavior at room temperature are one of those factors. Moreover, $BaTiO_3$ can be

fabricated as polycrystalline ceramics, single crystal and thin film, which is also a remarkable feature.

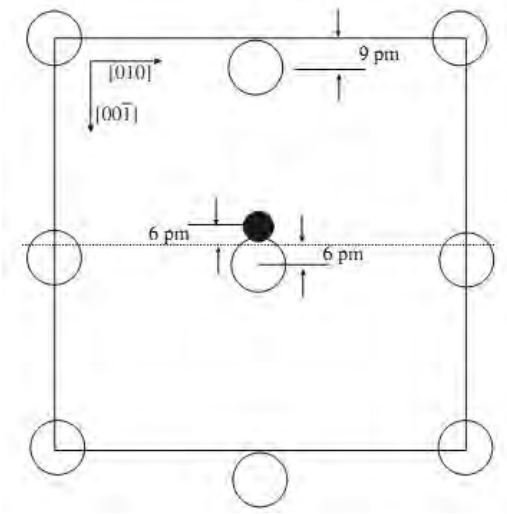

Figure 2.11: [100] Projection of Barium Titanate Showing the Ion Displacement below θc or Curie Temperature [7]

Having the point group of m3m, $BaTiO_3$ is cubic in nature above the Curie temperature (θ_C) as shown in Figure 2.10. Each barium ion is surrounded by 12 nearest neighbor oxygen ions. Each Ti ion has six oxygen neighbors. Barium and oxygen ions form a face centered cubic structure with titanium ion locating in the octahedral hole. The titanium ion is quite small in comparison to the octahedral hole. In comparison to the large Ba^{2+} ions (rBa^{2+} = 0.136 nm), the Ti^{4+} ion (rTi^{4+} = 0.064 nm) provides a radius ratio with oxygen of rTi^{4+}/rO^{2-} = 0.44. This value is close to the limiting value (≥0.414) for a coordination number of 6. That is why, titanium ion often finds itself in an off centered position. Therefore, it is sometimes referred as the "rattling" titanium ion. The direction of off-centering may be along one of the six <001> directions, or one of the eight <111> directions, or one of the twelve <110>directions as shown in Figure 2.11. This possible number of directions becomes limited below the Curie temperature. The calculation of dipole moment for $BaTiO_3$ can be done by using equation $\mu = qd$, where μ is dipole moment, q is the product of charge and ion charge, and d is the separation of positive and negative end of the dipole [7]. The dipole moment of the constituents of $BaTiO_3$ is given below

$$\mu(Ti^{4+}): (1.602 \times 10^{-19}\ C)\ (4)\ (0.06 \times 10^{-8} cm)$$
$$= 3.84 \times 10^{-28}\ C.cm$$
$$\mu(O^{2-}\ top): (1.602 \times 10^{-19}\ C)\ (2)\ (0.09 \times 10^{-8} cm)$$
$$= 2.88 \times 10^{-28}\ C.cm$$
$$\mu(O^{2-}\ side): (1.602 \times 10^{-19}\ C)\ (2)\ (0.06 \times 10^{-8} cm)$$
$$= 1.92 \times 10^{-28}\ C.cm$$

Now considering the number of each of the type of ion per cell, there is a single Ti^{4+}/cell, there is a top-face O^{2-}/cell, and there are two side-face O^{2-}/cell. Therefore, the total dipole moment per unit cell is

$$\mu = \mu(Ti^{4+}) + \mu(O^{2-} \text{ top}) + 2\mu(O^{2-} \text{ side})$$

$$= 1.056 \times 10^{-27} \text{ C.cm [7]}$$

2.10.1 Effect of Temperature on Structural Change of $BaTiO_3$

$BaTiO_3$ has got two basic structures; ferroelectric perovskite and non ferroelectric hexagonal which is stable above 1460°C [10] and metastably can stay in room temperature. At 1460°C hexagonal changes to cubic perovskite structure which is the basic ceramic product.

On cooling, the barium titanate structure changes from cubic to tetragonal perovskite structure below the Curie temperature which is 120°C, with a dipole moment along the c axis. The c/a ratio becomes more than one in this regards. Such changes favor the formation of ferroelectricity. Centro symmetric cubic structure transforms into tetragonal polar one. Ion displacement along with transformations' magnitude and direction is shown in Figure 2.12.

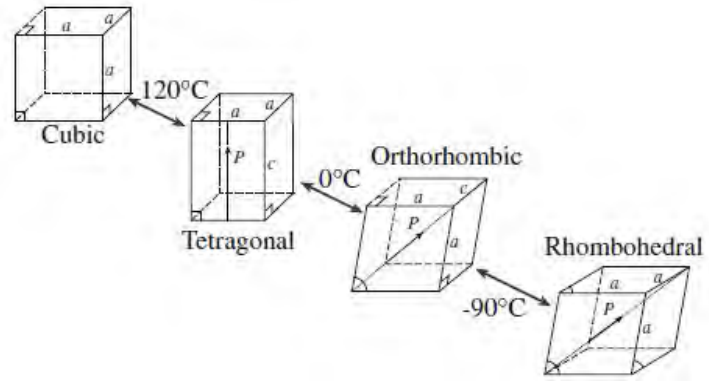

Figure 2.12 Polymorphic Transitions in $BaTiO_3$ [7]

Further cooling below subzero temperature, another polymorphic transformation occurs. The structure becomes pseudo monoclinic more precisely, orthorhombic. The third transformation occurs at -90°C. Orthorhombic structure transforms into rhombohedral structure, where the polar axis aligns along body diagonal with titanium shift along [111] direction [7].

2.10.2 Curie Point

All ferroelectric materials face temperature transition related to ferroelectric behavior. This temperature is called Curie temperature (θ_c) above which, material does not show ferroelectricity but below this value, material offers ferroelectric behavior. There is possibility where more than one ferroelectric phase may exist. Therefore, the temperature where ferroelectric transition occurs is called transition

temperature. The main change that occurs at the transition temperature is the change of crystal structure. For barium titanate, cubic structure persists above 120°C where the octahedral titanium ion moves randomly in the octahedral hole due to thermal vibration. On the other hand, below 120°C, structure changes from cubic to tetragonal and the octahedral site gets distorted. As a result, the titanium ion moves to an off centered position. A permanent dipole results from these phenomena. This temperature is known as the Curie temperature for the crystal of barium titanate.

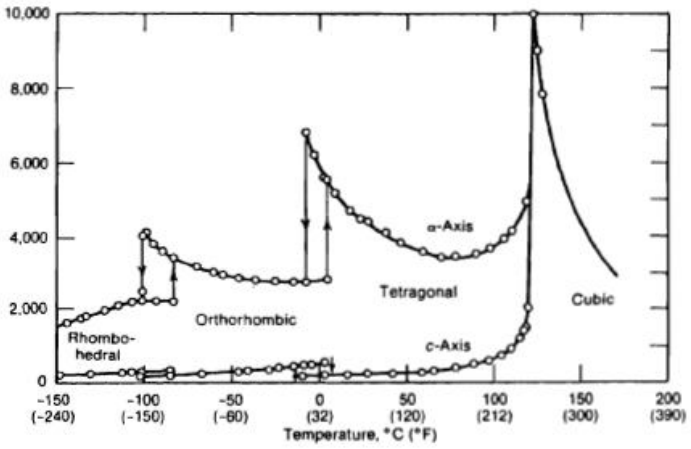

(a)

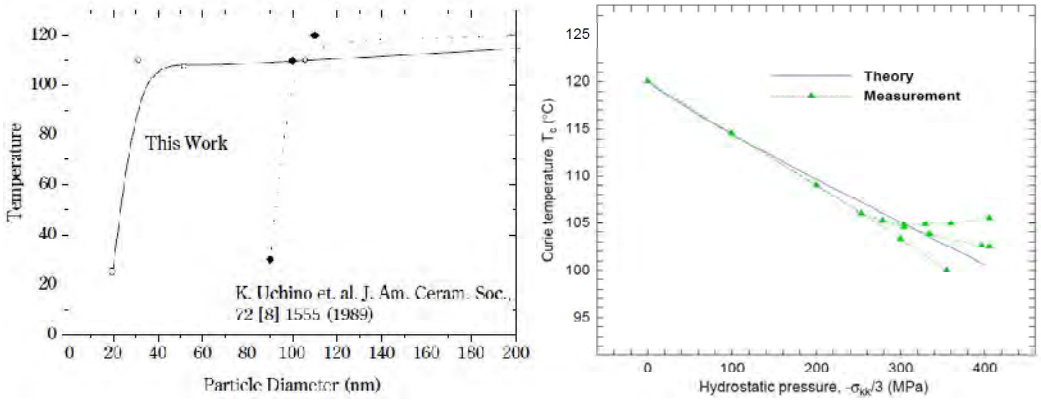

(b) (c)

Figure 2.13(a) $BaTiO_3$ Phase Change with Temperature [8], (b) Variation of Curie Temperature with Particle Diameter [11] , (c) Effect of Hydrostatic Pressure on Curie temperature of $BaTiO_3$ [12], respectively

Figure 2.13(a) shows the variation of dielectric constant with temperature, describing different crystal structure with corresponding temperatures. As both a and c axis data are available, below the Curie temperature, paraelectric cubic changes to ferroelectric tetragonal phases.

2.10.3 Shifting of Curie Point in Barium Titanate

Ohna and Suzuki [13] studied the size effect of ferroelectric materials on Curie temperature. Figure 2.13 (b) shows the effect of particle size effect on Curie temperature where shifting of Curie temperature towards lower side occurs with the lowering of particle size. They observed the particles corresponding to 20-30 nm, where drastic change in Curie temperature occurs for barium titanate. They mentioned about the lattice vibration that remained above the Curie temperature by secondary scattering. Similar trend has also been observed by Uchino *et al.* [11] measured by the change in lattice constant as a function of particle diameter. However the critical size was found around 100 nm instead of 20-30 nm. This change was attributed to the measurement techniques of particle diameter and crystal symmetry. Merz [14-18] has investigated the pressure dependence of transition temperature for barium titanium at a pressure range starting from 0 to 400 MPa and similar result was reproduced by Weng [12], where fall of transition temperature was observed with increasing pressure as shown in Figure 2.13 (c).

2.11 Production of $BaTiO_3$

Different methods are available for producing $BaTiO_3$. Bera *et al.* mentioned about the chemical processes, using barium oxalate and titanium di oxide precursors, in their work [19]. But some other routes are also available for the production of barium titanate especially when the powder size is in nano level. Barium titanate, nano sized with a narrow size distribution is always attracting for technical research as it is a good candidate for high capacitance capacitors [20]. Moreover, nano size materials always have higher surface energy enabling sintering at lower temperature, because the driving force for sintering is the reduction of total particle surface area [21]. Wet chemical process is a common methods however, needs high investment and precise process control. This forces to find alternative route of powder production [20]. Process of calcination starting with $BaCO_3$ and TiO_2 was studied by Manzoor *et. al.* [20] and Jamal *et. al*. [22]. A maximum calcination temperature of 900°C was used for the formation of $BaTiO_3$ for nano sized starting material. For micron size particle, same process was carried out at higher temperature due to larger particle size and lower surface energy. Even doped barium titanate has also been produced in the case of zirconium doping, where $Ba(Zr_{0.3}Ti_{0.7})O_3$ formation was reported with almost pure form of pervoskite structure at a calcination temperature of 1300°C [23]. Diffusion of Nb is slow in barium titanate when Nb is directly doped in $BaTiO_3$, so calcinations route may be an alternative to incorporate Nb into the octahedral site of $BaTiO_3$. Furthermore, industrially, this solid state route is still one of the economically viable processes over other wet processes. In this work, the same approach was taken for the production of Nb doped $BaTiO_3$.

2.12 Composition Analysis and Effects of Niobium (Nb) Doping

As mentioned earlier (section 2.10), barium titanate possesses ABO_3 type perovskite structure, and lots of efforts have been made to establish this structure. From the structural aspect, both A and B position can be substituted by different ions which could bring wide range of modification in the properties of barium titanate [24]. Having good dielectric properties, such substitution can bring significant change in the structure and properties of barium titanate in microscopic level. For example, as a donor dopant Nb has a valance of 5 which is quite different from that of barium or titanium ions. This can produce a charge imbalance and charge compensation that would result electron, hole or vacancies. Tetragonality of $BaTiO_3$ can be modified by introducing niobium (Nb) as a dopant [24]. Nb^{5+} has a ionic radius of 0.69 Å which is nearly equal to that of Ti^{4+}0.68 Å. In this case, it may increase the unit cell volume and decrease the tetragonality factor. By niobium doping, higher concentration of various defects is generated influencing the change in lattice parameter of the crystal structure of barium titanate. Furthermore, upon doping, Nb replaces the octahedral Ti ions and thus, raising the mobility of charge inside the material resulting high capacitance. This occurs due to the imbalance of charge as niobium has 5+ where as titanium has 4+ valance numbers. In this case, an excess of an extra +1 charge sustain from the balance of equation from tetravalent Ti ion and pentavalent Nb ion. At the same time, Nb can introduce strong polarization and thus, higher permittivity for having higher charge content instead of Ti ion in the octahedral position. However, the replacement of Ti by Nb in the octahedral hole must be ensured.

Niobium also plays an important role in inhibiting grain growth of barium titanate when it is doped in. Core-shell structure may form due to the low diffusivity of niobium into barium titanate. The coefficient of thermal expansion of shell is greater than the core. During heating, the core becomes in tension and shell in compression. This raises an internal stress in the structure which is quite large and increases with increasing niobium content. One of the main reasons for shifting of Curie temperature towards lower temperature has also been attributed to this internal stress for core-shell structure.

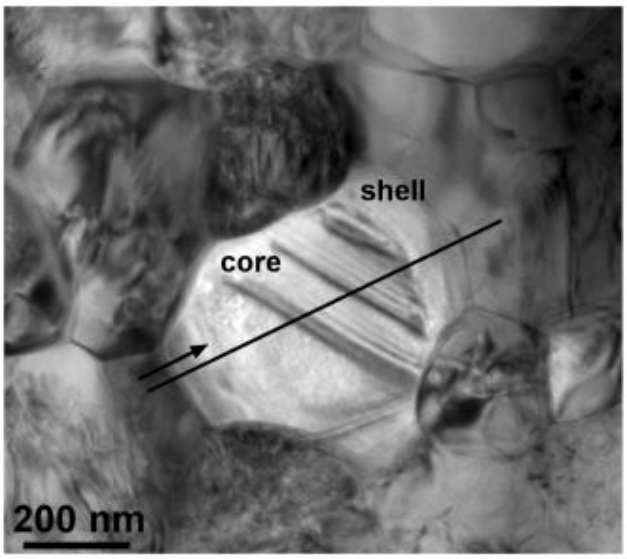

Figure 2.14 TEM Image of Core-shell Structure [25]

There are some discrepancies regarding the shifting of Curie temperature. Lowering of Curie temperature with increasing niobium content was reported by Yeon Jung Kim *et. al.* [26], contrarily, rising of Curie temperature with increasing niobium content has also been mentioned by Y. Yuan *et. al.* [27]. Further research is required in order to resolve this issue.

2.13 Effects of Grain Size on Dielectric Properties

Grain size determines the dielectric properties of barium titanate very strongly. It is believed that, reduction of grain size improves the dielectric constant [28, 29] and also reduces the dielectric losses [4]. Grain size depends on the initial particle size, sintering parameters like sintering temperatures, soaking time, heating and cooling rate, and sintering cycle design. Sintering can be done in either single stage or double stage. The main aim of the double stage sintering is to increase density without subsequent grain growth [30]. Various processing techniques have been practiced so far in order to produce fine grain structure with short sintering time [31]. Therefore, final grain size is fully dependent on sintering cycle.

During sintering, particles having different crystal space orientation, meet at point of contact and form grain, by grain boundary motion and finally ends up with one single grain. The crystal changes from cubic to tetragonal by changing c/a ratio, which is also associated with some volume change. Single grain can offer some resistance from the surroundings to the changing volume as it may hold multiple domains having different crystal orientations. This seems, one out of two crystals, intends to change its dimension whereas, the other one does not try to change its dimension along the same direction of the previous one. This resistance may happen in all over the crystals,

which can hamper domain formation badly. With the increase in grain size, number of individual crystal increases, and due to the resistance as mentioned, less number of domains is generated. Therefore, coarse grain formation is always unwanted for barium titanate based ceramics, as it has harmful effects on final dielectric properties. On the other hand, in fine grain structure, number of distinctive crystal it holds inside the grain, is smaller than coarse-grain structure. With the decrease in grain size, resistance on individual grains for changing the c/a ratio, becomes much less across the grain. Therefore, at transition temperature, cubic to tetragonal transition can take place easily, due to the low resistance for finer grain size, and easy dimension change for domain formation.

2.14 Domain Walls Motion with Electric Field

The motion of domain wall in ferroelectric such as barium titanate is quite complicated. Under an applied electric field a 180° wall in barium titanate move by repeated nucleation of steps by thermal fluctuations along the parent wall. Domain oriented by an angle of 180° can easily move than 90° domain wall as no physical motion is involved here. Motion of 90° domain wall is restricted by the strain involving the switching of c and a axis. The growth of ferroelectric domain under an applied field is shown in Figure 2.15.

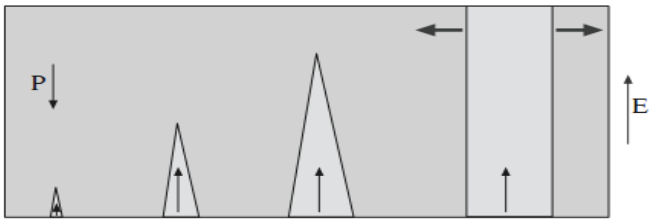

Figure 2.15. Growth of Ferroelectric Domain under Applied Field [7]

In the hysteresis loop, the horizontal portion indicates the saturated state where the crystal is a single domain during the cycle. Domain wall movement is restricted by defects and internal stress. Domain wall movement decreases with time even in absence of electrical, mechanical or thermal changes. Internal fields are associated with charged defects, redistribution of lattice strains and accumulation of defects at domain wall. Hysteresis loop is also a function of temperature which is shown in Figure 2.16.

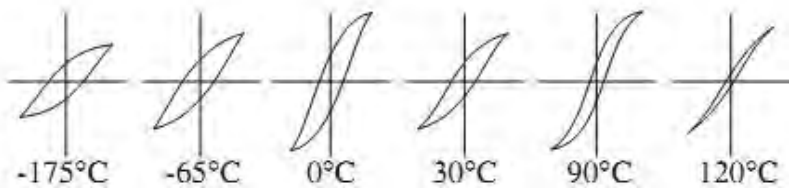

Figure 2.16 Hysteresis loop for Barium titanate as a function of temperature [7]

At low temperatures curves are flatter and E_c is greater representing higher energy requirement for domain orientation. With increasing temperature E_c decreases until θc where hysteresis loop is lost and material becomes paraelectric.

2.15 Application

Barium titanate is one of the most widely used materials in the field of electro ceramics. It is used as piezoelectric, ferroelectric, pyroelectric material in the practical field. Being a good dielectric material, $BaTiO_3$ has diversified uses in the field of capacitors. Capacitors generally have two groups; single layer capacitor and multilayer capacitor. In single layer capacitor, the construction has already been mentioned (section 2.2) with a dielectric placed at the centre of the two metallic electrodes. As the dielectric layer thickness is considerably high, they capacitance is lower for single layer capacitors. On the other hand, in multilayer capacitors, dielectric layer thickness is thinner with multiple layers which increase the capacitance of the capacitor to a greater extent. A schematic of multilayer ceramic capacitor or MLCC is given in Figure 2.17. Advanced tape casting technology has made it possible to fabricate MLCCs with less than 20 micron thick dielectrics. Property requirements for MLCCs are shown in Table 2.1, among which, X7R needs dielectric constant of 3000 having grain size around 1 micron which is one of the points of interest.

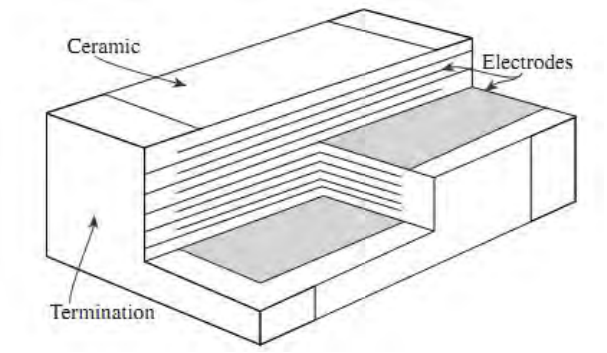

Figure 2.17 Multilayer Ceramic Capacitor [7]

Table2.1 Barium Titanate Based Dielectrics for MLCs [32]

Designation	Class	Temperature Range °C	Temp-Cap Change	Dielectric Constant upto	$BaTiO_3$ Content %	Other Ingredients	Grain Size
"Temperature Compensation"	1	-55 to +125					
NP0			±30ppm	75	10 to 50	$CaTiO_3TiO_2$ Rare Earth Oxides etc.	1µm
Intermediate K	2	-55 to +125					
BX, X7R			±15%	3000	90 to 98	Donor Dopants, Sintering Aids	1µm

High K	2	+1050 +85					
Z5U			+22% 56%	8000	80 to 94	Curie Point Shifters, Electrical Dopants, Sintering Aids	3-20 µm
Z5V			+22% 82%	18000	80 to 94		

2.16 Processing of $BaTiO_3$ Based Ceramics

Processing route plays an important role in determining the ultimate property of barium titanate based ceramics. Different processing routes can be used for fabricating such products. Sol-gel precipitation, chemical precipitation and hydrothermal-combustion are some of the major routes of fabrication. Optimum route totally depends on applications. But from the industrial point of view, the process of calcination by using barium carbonate and titanium dioxide at high temperature is still most popular. This is also known as solid state processing route. This method may not be appropriate for MLCCs as thin dielectric layer is required. Milling barium titanate in water can leach the barium ion and increase pH which is detrimental for further processing. Other chemical routes are expensive than solid state route and have different drawbacks. Hydro thermal synthesis, solution precipitation methods can involve hydroxyl group which may lead to porosity formation during sintering of MLCCs. So scientifically and practically, solid state route via calcination in order to produce barium titanate doped with Nb with narrow size distribution is a great point of interest for research.

2.16.1 Ball Milling

Ball Milling is one of the major steps in the processing of ceramics in solid oxide route. Raw materials like $BaCO_3$, TiO_2 and Nb_2O_5 can be mixed in a ball mill or pot mill. Milling is done not only for mixing the raw materials homogenously but also for breaking the agglomeration of particles and also for reducing their size to some extent. The schematic of ball milling is shown in Figure 2.18. The overall effect of ball milling ensures the mixing and doping of ions. Diffusion controlled solid state reaction is eased up for finer particles and homogeneity of particles resulted from ball milling. Previously, hardened steel balls were used for ball milling but for electronic ceramics, this can contaminate the mixture.

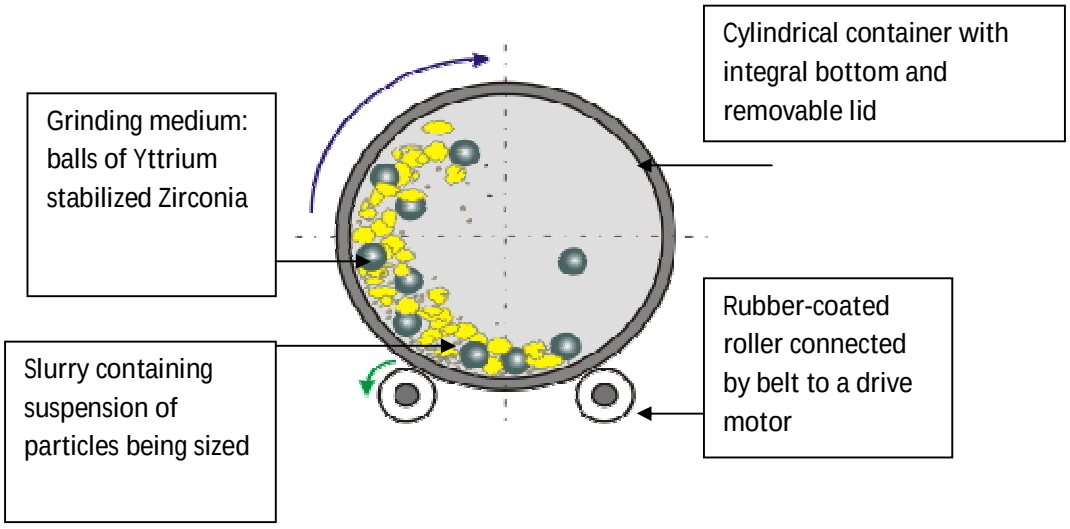

Figure 2.18 Ball Milling [33]

Furthermore, iron has detrimental effects on dielectric properties of barium titanate. As a result, ball of similar group of materials is necessary to avoid contamination. For this reason the Y_2O_3 stabilized ZrO_2 balls are now used in high density polyethylene (HDPE) pot for ball milling. Milling medium is another important issue when wet milling is concerned. The milling media must not react with the powders, pot and the balls. It also needs to avoid the decrease of colloidal stability. Water as milling media can react with barium titanate in a tribochemical reaction and forms $Ba(OH)_2$ which is completely unwanted. This can decrease the colloidal stability of the suspension. Non polar liquid such as acetone, alcohol can be used in this regards. Similar setup is used for the milling after calcinations with reduced amount of milling time. Finally, evaporation of milling media is mandatory to proceed for further processing like pressing and sintering.

2.16.2 Pressing and Drying

Milling is must before and after calcinations in order to ensure homogenous mixing of both raw materials and calcined product. The milled powder after calcination is given certain shape for further processing which is termed as green body. In order to give shape, binder like PVA or poly vinyl alcohol is mixed with powders to hold the shape of the body for further handling. The green body has to obtain certain density before they are suitable for sintering. Generally, 60% of the theoretical density should be achieved in pressing before sintering. Different techniques are available for giving desired shape and density prior sintering. Powder compaction, slip-casting, extrusion, doctor's blading, dipping are some of the available forming techniques. Hot press is another popular method of ceramics processing. Though it is expensive, it is suitable for high end application. The choice of process is fully dependent on powder type, particle size, size distribution, agglomeration, desired shape of product and final thickness of product. In powder compaction method, hydraulic press is used with a

pressure range of 100 to 300 MPa. Simple and symmetric shape can be pressed via this method and no sintering aid is added as it is solid state sintering. Only PVA binder is added as mentioned earlier, to obtain the green strength of the powder compact, which is essential for handing for further processing like sintering.

During sintering an intermediate heating stage is necessary near about 400-600^{o}C in order to remove the binder from the ceramic body. Careful and slow heating rate is necessary in this stage so that, evolved gases emitted from the ceramic body due to the burning of binder, can come out easily from the ceramic body without causing any cracks or blisters. After this burnout, ceramic body is heated to higher temperature for sintering.

2.16.3 Sintering

Densification of a particulate ceramic body using heat is termed as sintering. During sintering removal of pores occurs among the starting particles associated with the shrinkage of the ceramics body. In addition to that, growth and bond between adjacent particles also occur simultaneously. There are some factors that must be present during sintering such as mechanism of material transport, source of energy to initiate and sustain the material transport. There are six transport mechanisms so far identified in case of sintering; surface diffusion, volume diffusion, evaporation-condensation, grain boundary diffusion, volume diffusion and plastic flow [7]. However, the primary mechanism of transport is diffusion and viscous flow. The main source of energy is heat in association with energy gradient due to contact between particles and surface tension. All the properties of ceramic body is directly related to the structure of the sintered mass which is a strong function of sintering parameters like heating rate, sintering temperature, soaking period, cooling rate, atmosphere etc. Different types of sintering techniques are available for ceramics processing but in this case discussions will be concentrated only on solid state sintering process. In the process of sintering inter granular bond is developed between adjacent powder particles by surface diffusion and other mechanisms that has been discussed earlier. The green density of ceramics body starts to increase during the sintering process when heat is applied and more particles are bonded with each other. Having 80-90% of the theoretical density, the pores in the ceramic mass are still open and dielectric constant value measured is very low. Furthermore, Curie temperature is also pronounced weakly. Closing of pores occurs nearly at 95% of the theoretical density of the mass. More heat can improve density values by issuing out the trapped gases along the grain boundaries. Density below 95% of theoretical density, may result the existence of open pores that would cause dielectric loss and poor dielectric properties. Choosing the optimum sintering temperature is a tricky part of the experiment. Low temperature sintering may result ceramic mass of poor density, on the other hand, high temperature more than required, may produce structure with very coarse grain that may result low dielectric properties. So the only method of producing dense

ceramic body without abnormal grain growth is firing the ceramic body with optimized sintering temperatures and parameters. And optimization can be done by trial and error method depending on various process parameters and compositions.

2.17 Recent Works on Barium Titanate Ceramics

Barium Titanate has been one of the most widely studied dielectrics in the field of ceramics. Scientists have been working on the production, processing techniques, structure property relationships and temperature dependent behavior of $BaTiO_3$.

In 2001, S. Garcí´a *et. al.* studied the doping behavior of $Sr_{0.3}Ba_{0.7}Ti_{(1-5y/4)}Nb_yO_3$ with different doping concentration. Lowering of grain size with increasing Nb concentration was observed. In his work, the product was prepared through the process of calcination. With increasing Nb concentration the transition temperature was found lowering linearly. This behavior was attributed to the fact of degree of disorder having two ions occupying same lattice site. Broadening and shift of transition temperature towards lower temperature has also been attributed to this disorder.

Wen Li *et. al* studied the doping behavior of Nb_2O_5 and Co_2O_3 in temperature stable $BaTiO_3$ based ceramics in 2002, where the dopant concentration was varied from 0.3 to 0.7 wt.%. In addition to that, CeO_2 and Sm_2O_3 were also added to the mixture with varying amount of concentration. Nb_2O_5 and Co_2O_3 were found effective to enhance the dielectric constant of material with whole temperature range of X7R specifications.

B.D. Stojanovic along with his colleagues worked on the size effect on structure and dielectric properties of Nb doped barium titanate in 2003. A remarkable phenomenon was mentioned in this work, when grain size becomes less than 700 nm or 0.7 microns, barium titanate structure converts from tetragonal to pseudocubic, and dielectric values becomes very low. In case of doping, this effect is more complex. Dielectric constant below 1000 at room temperature was reported in this work for Nb doped $BaTiO_3$ samples, which is quite low.

Xiaoxing Wang *et. al.* in 2004 studied the positive temperature coefficient of resistivity (PTCR) effect of Nb doped barium titanate. The sintering temperature was lowered by adding YB_6 below 1200°C. Good PTCR properties were observed for $BaTiO_3$ doped with 0.2 mol% Nb_2O_5 and 1 mol% YB_6 sintered at 1150°C.

Another aspect of niobium oxide, barium oxide and titanium oxide system, is application of the system in the field of low loss microwave dielectric ceramics. $BaTiNb_4O_{13}$, $BaTiTa_2Nb_2O_{13}$, $BaTiTa_4O_{13}$, $Ba_3Ti_4Nb_4O_{21}$, $Ba_3Ti_4Ta_4O_{21}$, $Ba_3Ti_5Nb_6O_{28}$, $Ba_3Ti_5Ta_6O_{28}$ and $Ba_3Ti_5Nb_3Ta_3O_{28}$ were prepared by M. T. Sebastian in 1999 as low loss microwave dielectric materials. Process of calcinations was used from 1200 to

1300°C in order to obtain the desired products. Required permittivity (less than 100), high Q and small T_f were observed for developed materials, which have potential applications for microelectronics. Substitution of Ta in $BaTiNb_4O_{13}$, $Ba_3Ti_4Nb_4O_{21}$ was found effective in obtaining wider dielectric constant range.

In 2006, N. Maso´ and his colleagues processed and characterized the electrical properties of Nb doped barium titanate. Comparative study between two methods was performed; solid state reactions at 1500°C and sol-gel synthesis from high purity alkoxide precursors with final heat treatment at 900°C. $BaTi_{1-5x}Nb_{4x}O_3$ ($0 \leq x \leq 0.075$) being the base formula, was chosen for solid state route and, $0 \leq x \leq 0.015$ was chosen for sol-gel route. In this work, it was suggested that sol-gel method of processing, is much more efficient in achieving homogenous structure whereas, in solid state route, it would rather take several days to obtain homogeneity. Difficulty of homogenization of multivalent cations Ti^{4+} and Nb^{5+} have been claimed responsible for such sluggishness of solid state reactions even at 1500°C. Electrical properties for samples fired at 900°C for 12 hours, was found highly insulating, indicating no existence of electronic compensation mechanisms which may be attributed to oxygen loss or direct donor doping. This was also reported that, mechanism of charge compensation by introducing Nb into the $BaTiO_3$ lattice may create of titanium vacancies into the lattice.

Bin Cui *et. al.* prepared and characterized niobium doped barium titanate nanocrystalline powders and ceramics in 2007. Lowering of grain size and Curie temperature were reported in this work due to the addition of Nb.

In 2009, Asad Jamal and others prepared barium titanate through the process of calcination, by calcining powder mixtures at 900°C on the basis of TG/DTA studies. Percent weight loss was reported higher than reported in the contemporary literatures. Moreover, 900°C of calcination temperature was reported insufficient to produce desired product as secondary phases of untransformed $BaCO_3$ and Ba_2TiO_4 were detected.

Microstructural characterization and dielectric properties of donor doped barium titanate was studied by Yeon Jung Kim *et. al*. in 2009. Niobium and tantalum were used as dopants for the work. Low dielectric constant was reported even after the addition Nb in barium titanate which happened to be around 2000-3000. Local structure around Ti^{4+} was not affected by the addition of Nb and/or Ta. Furthermore, the local structure was claimed pseudocubic or rhombohedral. Lowering of Curie temperature was also observed with the addition of dopants comparing with pure barium titanate.

Also in 2009, Y. Yuan along with his associates, studied Nb doped barium titanate along with microstructure and dielectric properties. Secondary phases were detected

by XRD when Nb_2O_5 concentration exceeds 1.2 mol%. Shift of Curie temperature towards higher side was reported in this work with the addition of Nb which is contrary to the other works, that have so far been reported. This was attributed to the formation of large internal stress, rising from the misfit of core and shell of core shell structure, and also due to the formation of large grained secondary phases.

In 2011, several works were done on barium titanate specially, doped with niobium. Yunxia Zhang and his colleagues claimed the formation of perfectly crystallized grains. Moreover, effective flattening of dielectric constant k vs temperature curve was also reported.

T. Dechakupt and others investigated the $(BaTi_{1-x}Nb_x)O_3$, x = 0 to 0.02 via mix oxide route through the process of calcination. Lowering of grain size with increasing Nb content and shifting of Curie temperature towards lower side were reported in this work. However, the transformation mechanism of barium titanate from semiconducting to insulating with increasing Nb content was not clarified in this work. Furthermore, discrepancies relating to the shifting of Curie temperature with Nb addition have been mentioned in this work which is still to be resolved.

In 2013, Pat Sooksaen *et. al.* worked on high Nb content in barium titanate, where sample containing more than 0.9 mol% Nb_2O_5 resulted the formation of needle like second phase. The facts related grain size was found consistent with previous literature. But facts related shifting of Curie temperature with dopant concentration was not made clear.

Chapter 3

Experiment Processes

3.1 Raw Materials

In this work, niobium doped barium titanate was prepared via mixed oxide route through the process of calcination. $BaCO_3$, TiO_2 and Nb_2O_5 were used in powder form as raw materials. The detailed description of the powder materials are given below and tabulated in Table 3.1.

Barium Carbonate ($BaCO_3$)

Purity: 99.8%
Particle Size: 800nm
ID: US3817

Titanium Di Oxide (TiO_2)

Purity: 99.9%
Inframat Advanced Materials
ID: IAM101943AT

Niobium (V) Oxide (Nb_2O_5)

Purity: 99.9%
Inframat Advanced Materials
ID: 41R-0804

Binder: Poly Vinyl Alcohol (PVA)

Degree of polarization = 1700 to 1800
Hydrolysis = 98-99
Volatiles = 5% Max
Ash Content = 0.7%
pH of Water = 5-7

Table 3.1 Properties of Components

Components	Atomic Number	Atomic Weight	Molecular Weight	Density (gm/cc)
Barium (Ba)	56	137.33	-	3.51
Niobium (Nb)	41	92.90	-	8.57

Components	Atomic Number	Atomic Weight	Molecular Weight	Density (gm/cc)
Titanium (Ti)	22	47.86	-	4.506
Barium Carbonate ($BaCO_3$)	-	-	197.34	4.286
Barium Titanate($BaTiO_3$)	-	-	233.19	6.02
Niobium oxide (Nb_2O_5)	-	-	265.81	4.60
Titanium Dioxide (TiO_2) Anatase	-	-	79.866	3.78

3.2 Preparation of Samples

Initially, all the raw materials ($BaCO_3$, TiO_2 and Nb_2O_5) were mixed and milled. As the main objective of this work was to produce Nb doped $BaTiO_3$ through the process of calcination, milling was done prior to calcination. After calcination, powders were milled again to homogenize the calcined mass. Initial batch was made around 20 grams. But batches of different weight have also been prepared according to the requirement of prepared sample. Batch compositions also varied with different doping level of niobium. After calcinations, powder were pressed, sintered and then final characterization was performed.

Table 3.2 Formulations of Samples at Different Doping Level

Doping level	Powder	Weight Percent of Powder in Batch
0.4 mol% Nb	$BaCO_3$	72.1293
	TiO_2	28.6790
	Nb_2O_5	0.19166
0.8 mol% Nb	$BaCO_3$	71.07521
	TiO_2	28.54176
	Nb_2O_5	0.383035
1.6 mol% Nb	$BaCO_3$	70.96646
	TiO_2	28.26864
	Nb_2O_5	0.764898

3.2.1 Weighing of Samples

According to the percentage, different batches were prepared for different doping level. Typical batches were of 20 grams as mentioned earlier. Powders were weighed in high precision electronic balance in order to ensure the accuracy of doping.

3.2.2 Ball Milling

Powders having different composition in relation with doping level were taken in laboratory pot mill containing Yttria (Y_2O_3) stabilized zirconia ball with acetone as milling media. Two types of balls were used in ball mill; having the diameter of 3 mm and 5 mm. All the balls and the pots were cleaned as perfectly as possible followed by ultrasonic cleaning so that slightest of foreign particle was not present there which may come up in the final structure and deteriorating the dielectric and other relevant properties. The powders were at the top of the balls in the pot and acetone was added in a sufficient way. Then the pots were capped tightly, the mixture was mixed by shaking and then powders were milled by rolling the pot over rubber coated shaft, driven by electronic motor at moderate rpm. Rotation of the mill must be moderate so that balls inside the pot can get a certain level of elevation and can drop on the powder mixture in order to pulverize and mix the same. Milling was carried out for period of 18-20 hours. After ball milling powder mixtures were completely dried and calcined. After calcination, powders were milled again for six hours with the same setup. Then powders were completely dried in order to remove the acetone and moistures. Then it was taken for adding binder and pressing.

3.2.3 Calcination

Calcination is an important part of this research. Barium carbonate, titanium dioxide and niobium oxide were calcined according to different composition corresponding to different doping level. Basic reaction during calcination is stated as follows:

$$BaCO_3 + (1-x)\ TiO_2 + x/2\ Nb_2O_5 = (BaTi_{(1-x)}Nb_x)O_3 + CO_2 \ ;\ x=0.004 = 0.4 \text{ mol\% Nb}$$

$$x=0.008 = 0.8 \text{ mol\% Nb}$$

$$x = 0.016 = 1.6 \text{ mol\% Nb}$$

The calcination of the powders were performed at 1300°C for 2 hours and this temperature was chosen on the basis of literature review and MSDS data sheet of barium carbonate where barium carbonate decomposes. The calcination cycle is shown in Figure 3.1 where reaction occurred and niobium doped barium titanate formed. The detailed of this will be discussed in next chapter.

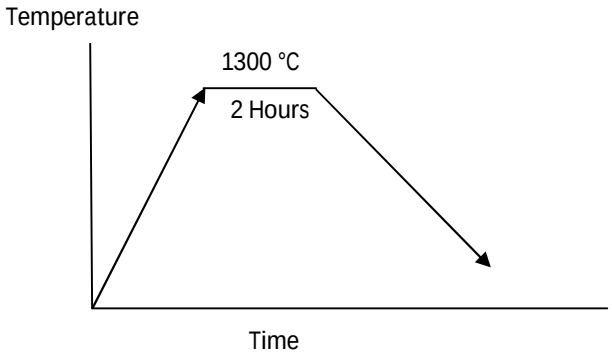

Figure 3.1 Calcination Cycle

3.2.4 Binder Preparation

Generally, polyvinyl alcohol or PVA is added to the powder mixture in order to hold the particles together when it is pressed. Certain steps were followed in order to prepare binder. 3-3.5 gm of PVA was added in 50 cc of distilled water in a beaker. The beaker was kept on hot plate and was stirred continuously. Stirring was performed until all the PVA pellets got dissolved into the water and a thicker or viscous liquid was produced. Precautions were taken by keeping the temperature of the mixture below 80°C, and by continuous stirring in order to avoid the agglomeration of PVA.

3.2.5 Addition of Binder Prior to Pressing

After post calcination milling and drying, binder was added to the powders. Typically, 20 grams of samples require 2.0 gram of binder but this ratio is not fixed. During the addition of binder powders get agglomerated and a large mass of sticky powder is produced. So powder mixtures were continually stirred upon the addition of binder. Binder was added in small quantity rather than the whole amount altogether. To ensure the distribution of binder in powder, continuous stirring was performed. Moreover, to avoid the agglomeration of powder and absorption of moisture, the mixtures were kept in oven for 10-15 minutes at a temperature of 100°C in time to time during the course of binder mixing. Finally, a fine powder product with homogenously distributed binder was obtained and mixtures were ready for pressing.

3.2.6 Pressing

Before final pressing, powders were kept in drier at 100 °C for an hour so that all the absorbed moistures were completely removed. The pressing die having a diameter of 13 mm along with the press was cleaned. Then powders were pressed into pellets by applying a load of 2 ton approximately equivalent to a stress of 150 MPa.

After pressing, pellets having a diameter of 13 mm were obtained. Thickness of pellets was maintained around 2 mm in order to avoid density variation within the samples. A schematic of the pressed product is shown in Figure 3.2.

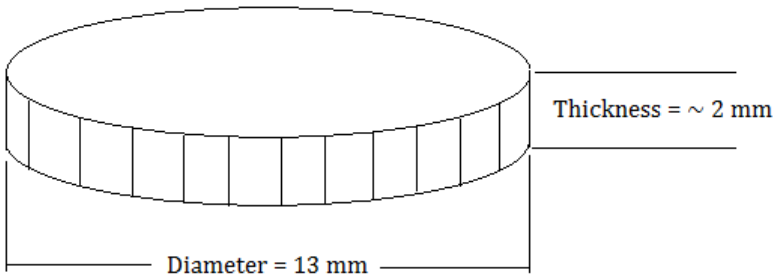

Figure 3.2 Schematic of Powder Compacts after Pressing

3.2.7 Drying

The pressed samples were kept in drying oven for a minimum period of 3 hours in order to remove all the moistures absorbed by the samples. Then the pressed samples were fully ready for sintering.

3.2.8 Binder Removal and Sintering

During sintering pellets were fired in a sintering furnace. In this work, high temperature furnace manufactured by Nabertherm was used.

It is important to have an intermediate soaking stage during sintering in order to remove the binder from the sample. Generally, PVA binder removes at a range from 400-500°C. Therefore, during the sintering cycle, an intermediate soaking period was included in order to remove the binder at 500°C with a soaking period of 1 hour. A slow heating rate of 3°C/min was applied to the sample during the binder removal stage, so that formations of cracks or blisters can be avoided.

After the removal of binder from the samples, temperature was raised to higher temperature to sinter the samples. Depending on composition, optimum sintering temperature as well as other sintering parameters such as heating rate, soaking period can vary. As a result, trial and error method was applied to find the optimum sintering parameters. In this work, sintering was performed at a range of 1350-1550°C for 2 hours of soaking time at the sintering temperature. The typical sintering cycle is shown in Figure 3.3.

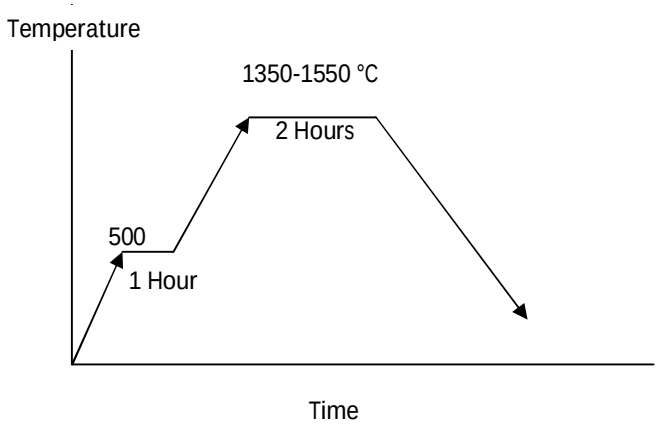

Figure 3.3 Sintering Cycle for Firing Ceramics Samples

Heating rate is an important issue after the binder removal stage. Higher heating rate 10°C/min can be used beyond binder removal stage. However, it was also optimized by trial and error method. Both 5 and 10°C/min of heating rate were used in this work. After soaking at the sintering temperature samples were cooled at a cooling rate of 3°C/min, which was quite slow and was chosen in order to avoid cracking due to faster cooling. After sintering, samples were ready for further characterizations.

3.3 Characterizations and Measurement of Properties

3.3.1 Percent Theoretical Density

After sintering the first property that was measured is the density of the sample and determining the percent theoretical density achieved after sintering. Density was determined by taking weight of the sample with high precision electronic balance and measuring the dimensions by using micrometer. Then weight of the sample was simply divided by volume obtained from dimensions of a particular geometry. The resultant densities were compared with theoretical density and were expressed in terms of percent theoretical density achieved. The theoretical densities of the samples for different doping level have been listed in Table 3.3.

Table 3.3 Theoretical Densities for Different Doping Level of Niobium

Compositions	Theoretical density
$BaTiO_3$ Doped with 0.4mol% Nb	6.0302 gm/cc
$BaTiO_3$ Doped with 0.8mol% Nb	6.0404 gm/cc
$BaTiO_3$ Doped with 1.6mol% Nb	6.0608 gm/cc

3.3.2 Microstructure Analysis

As sintered samples were meant to be observed under scanning electron microscope (SEM) and field emission scanning electron microscope (FESEM), no preparation was needed at this stage. As-sintered samples were used for microstructural analysis.

In this work, both SEM and FESEM were used in analyzing the microstructures depending on the availability and working conditions of the instruments. SEM manufactured by Philips and FESEM- JEOL JSM-7600F were used in this work. Moreover, for producing better images some samples were coated with gold by sputtering. EDS or energy dispersive spectroscopy on certain features of microstructures were also conducted by FESEM.

3.3.3 Particle Size Analysis

One of the main purposes of this work was to prepare niobium doped barium titanate powder through the process of calcination and characterizing the same after sintering. Therefore, main product was prepared via calcination and characterization of particle size distribution of both raw materials and calcined product was done by a laser based particle size analyzer (model microtrac-S3500). After calcination, powders were milled for six hours and subjected to particle size analysis. This is important, as these powders were meant to be sintered and final microstructure of the sample is a strong function of size and distribution of the raw materials.

3.3.4 X-Ray Diffraction

The only option available to confirm the formation of niobium doped barium titante having a perovskite structure was X-ray diffraction or XRD. After calcinations, samples having different doping level were analyzed by XRD. The phase analysis of this work was performed by Bruker D8 Advance diffractometer with $\lambda_{Cuk\alpha}$=1.5406 Å. Furthermore, lattice parameter like 'c' and 'a' values for differently doped samples were calculated by using Bragg's law: $2d\sin\theta=n\lambda$, where d is the spacing between the planes, θ is the angle between incident X-ray and scattering planes, λ is the wave length of the incident ray and n is an integer. By placing all the values from XRD patterns, d spacing was calculated. Using the value of d spacing, lattice parameters were calculated by using the formula: $d=a/\sqrt{(h^2+k^2+l^2)}$, where, a is lattice parameter and h, k, l are the Miller indices of the Bragg plane. Twin peaks in XRD provided two 2θ positions for different planes for tetragonal structure, which gave two d spacings. The d spacings with corresponding Miller indices resulted two values of lattice parameter; 'a' and 'c'.

3.3.5 Dielectric Characterizations

Dielectric properties of the samples were measured by using an impedance analyzer, Wayne Kerr 6500B series. However, before doing so prepared samples were painted with silver paste on both sides without painting the edges. Sample's geometry was also measured with micrometer or slide calipers. Then copper wires were attached to

both sides of the samples to connect them with the analyzer. Additionally, holder was used for connecting the samples with the analyzer and holding the same inside the furnace for high temperature measurements. Dielectric loss readings were collected directly from the analyzer but for dielectric constant, capacitance was measured and the following formula was used in calculating the dielectric constant (k).

$k=Cd/(A\varepsilon_0)$

k=Dielectric Constant
C=Capacitance
A=Area of the Sample in Contact with Conducting Layer
d=Thickness of the Sample
ε_0= Permittivity of Vacuum

3.3.6 XRF

XRF or X-ray fluorescence was performed on sample in order to check the consistency of calculated weight percentage and recovered weight percentage after sintering. XRF analysis was done by Lab Center, XRF 1800, Shimadzu.

3.3.7 Image Analysis

In this work, the grain size measurement from SEM or FESEM micrographs was performed by using Image J software package.

3.3.8 ANOVA Modeling

Analysis of variance (ANOVA) requires two sets of variables and a measured property on which the significance of variables can be studied. In this work, significance of Nb doping level and sintering temperature was studied on grain size and density respectively. In addition to that, holding time and frequencies' effects on dielectric constant of a particular composition was also observed. If 'A' and 'B' are the two variables with their high and low levels + and - and the measured property is 'Y', then AB which is the interaction of A and B must be determined. The basic calculation of ANOVA modeling is shown in Table 3.4 as an example.

Table 3.4 Calculation of ANOVA Modeling

%Nb (A)	Temperature °C (B)	A	B	AB
0.4	1425	-	-	+
0.4	1450	-	+	-
0.8	1425	+	-	-
0.8	1450	+	+	+

Significance of variables on measured properties can be projected via Pareto charts, where individual as well as collective effect of variables; A, B or AB on property Y can be shown. This can be constructed by multiplying the average value of Y with corresponding sign of A, B and AB and summing them up. This summation provides the Δ values. Finally, charts are constructed by ranking the Δ/2 values. ANOVA is not a technique of testing the difference between two sample variances but it is a technique to test the significance of differences among the sample means [34].

Chapter 4

Results and Discussion

4.1 Particle Size Analysis

Particle size of the samples was analyzed by particle size analyzer. Raw materials for calcination reaction; Barium carbonate, titanium dioxide and niobium(v)oxide, as well as calcined product, barium titanate containing 0.4, 0.8 and 1.6 mol% Nb were analyzed by particle size analyzer.

4.1.1 Particle Size Analysis of Raw materials

The particle size analysis of raw materials is shown in Figure 4.1, plotted with particle size in microns against their percentage of concentration corresponding to different sizes.

From Figure 4.1 (a), the size distribution appears to be very narrow for barium carbonate. It is also observed that, particle size ranged from 0.5 to 1 µm with a maximum occurrence of approximately 50% corresponding to the particle size of 0.7 µm. Larger size distributions of particles were found for TiO_2 and Nb_2O_5 as shown in Figures 4.1 (b) and (c) respectively. TiO_2 samples contained larger particle size in micron range with a narrow size distribution, however small percentage of particles can also be seen on the higher and lower side of distribution (Figure 4.1(b)). Wider size distribution, obtained for Nb_2O_5 particles provided two major peaks in the distribution curve; around 0.25 microns and 5 microns (Figure 4.1(c)). In addition, a considerable amount of particle was detected for different size, ranging from nano to micron size.

Overall, both micron and nano size particles were found in raw materials, used in this work.

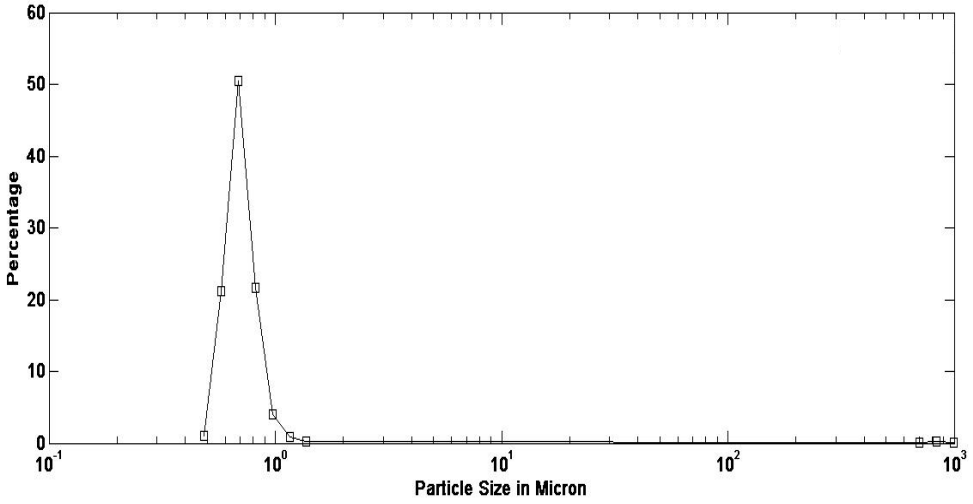

(a)

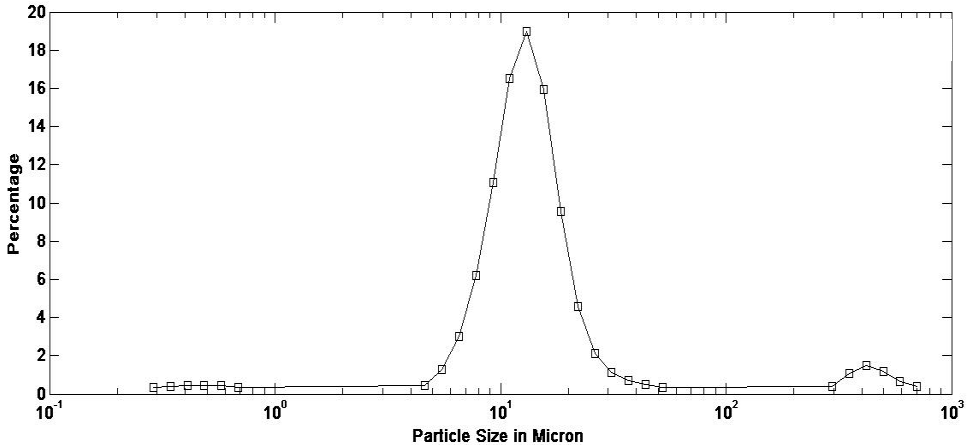

(b)

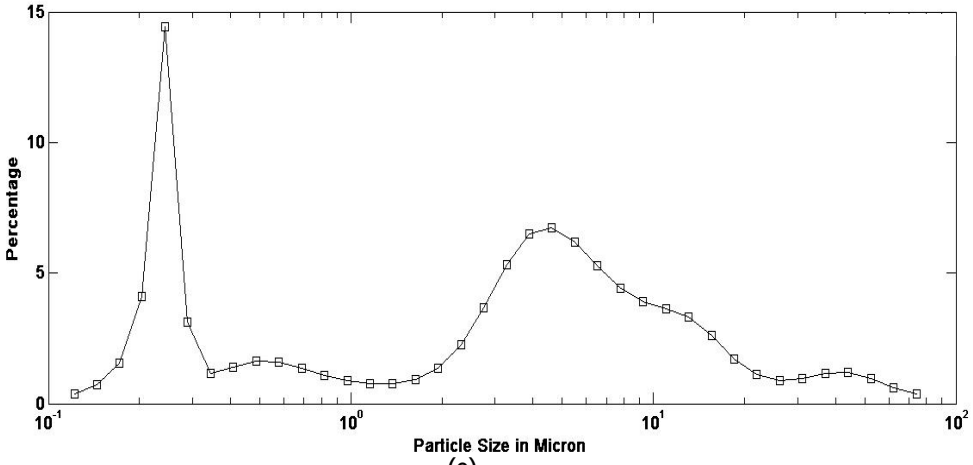

(c)

Figure 4.1 Particle Size Analysis of (a) Barium Carbonate, (b) Titanium dioxide and (c) Niobium (v) Oxide

4.1.2 Particle Size Analysis and FESEM of Calcined Product

When powders were mixed and calcined according to predetermined doping levels, a different particle size and distribution were found compared to the distribution of raw materials as shown in Figure 4.1. During calcination, raw materials having distinct particle sizes and distributions, reacted and formed Nb doped barium titanate with different size distributions. The distribution curves for all three calcined powders with FESEM images are shown in Figures. 4.2-4.4. For all the doping levels, bimodal distribution is observed. In addition, a small peak at higher range has also been observed for all three compositions.

By analyzing Figures 4.2-4.4, it can be visualized that particles much less than 1 µm were produced in each case of the calcined products for all three doping level. However, with the addition of Nb, particle size was decreased gradually. In addition, the coarser particles as projected in the higher side of the distribution curves, have not been observed in the micrographs which may occur due to the unbroken agglomeration of particles during particle size analysis. Furthermore, along with fine particles, some coarser particles were present in calcined product doped with 1.6 mol% Nb, which has not been observed for other doping concentrations. This may happen due to secondary phase formation for higher doping level of Nb compared to other compositions. Producing calcined powder much below than 1 micron can be considered as a good achievement as these powders were meant to be sintered later. Also, sub microns or particles even of few hundreds of nano meter are very much essential for producing microstructure having fine grain size when sintered. This fine grained structure may result good dielectric properties if fabricated appropriately.

In summary, for all doping concentrations, completely different particle size (bimodal) distributions were obtained after calcinations, compared to the principle constituents like $BaCO_3$, TiO_2 and Nb_2O_5. Moreover, consistencies in size distributions in calcined product have also been observed with similar trend in distribution curve.

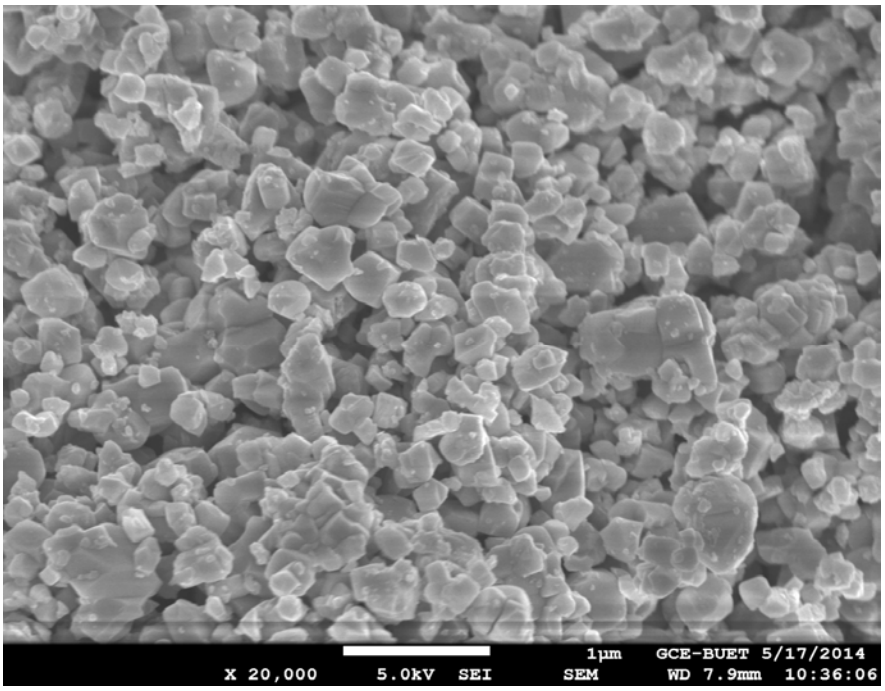

(a)

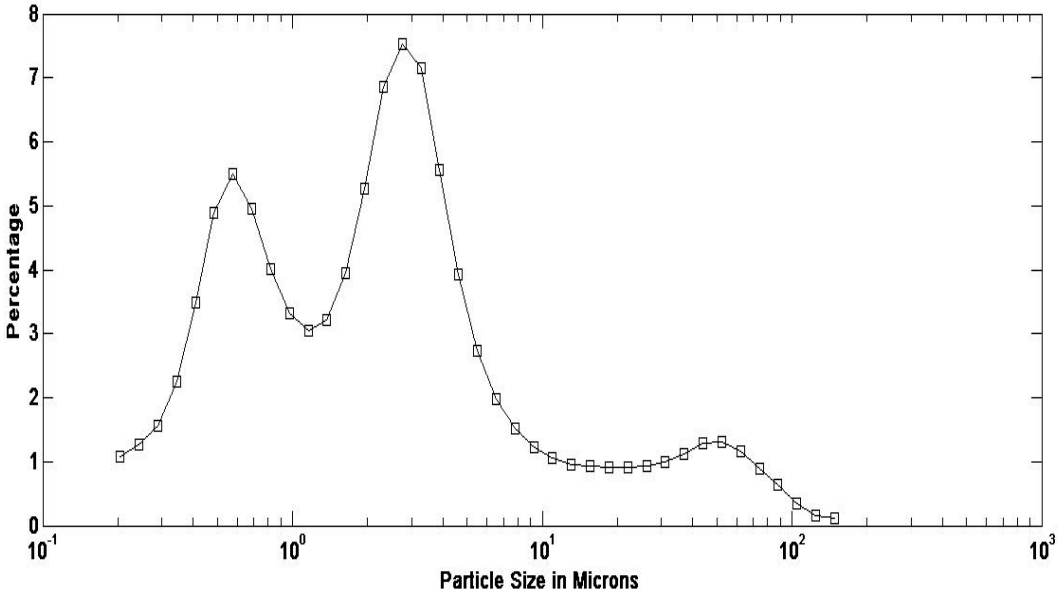

(b)

Figure 4.2 (a) FESEM Micrograph and (b) Corresponding Particle Size Analysis of 0.4 mol% Nb doped Sample

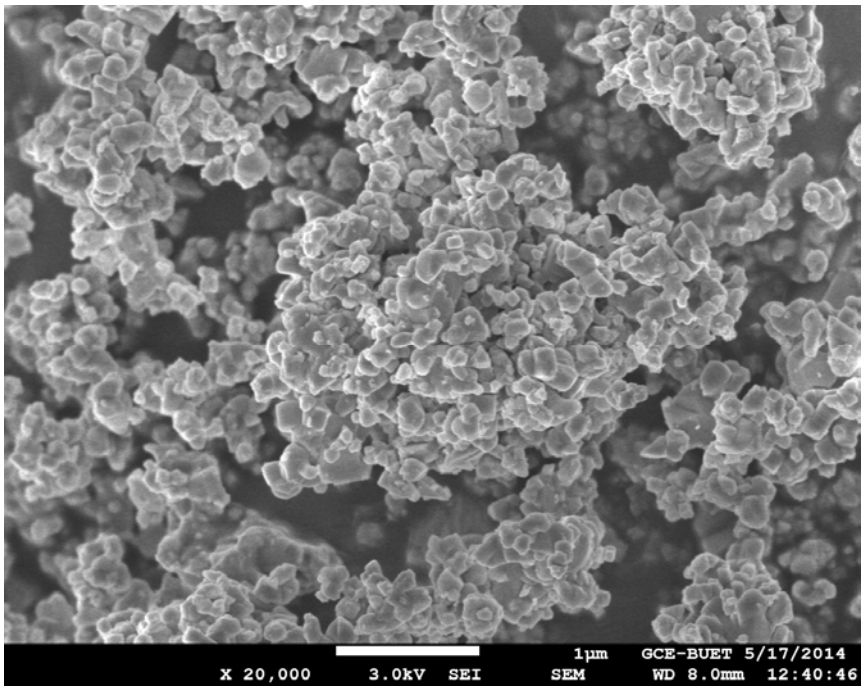

(a)

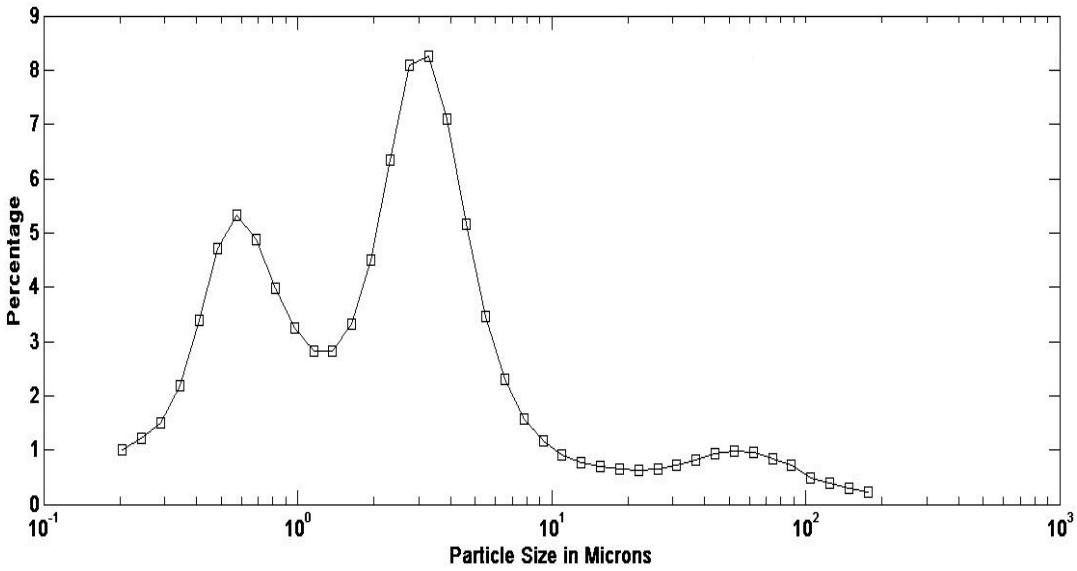

(b)

Figure 4.3 (a) FESEM Micrograph and (b) Corresponding Particle Size Analysis of 0.8 mol% Nb doped Sample

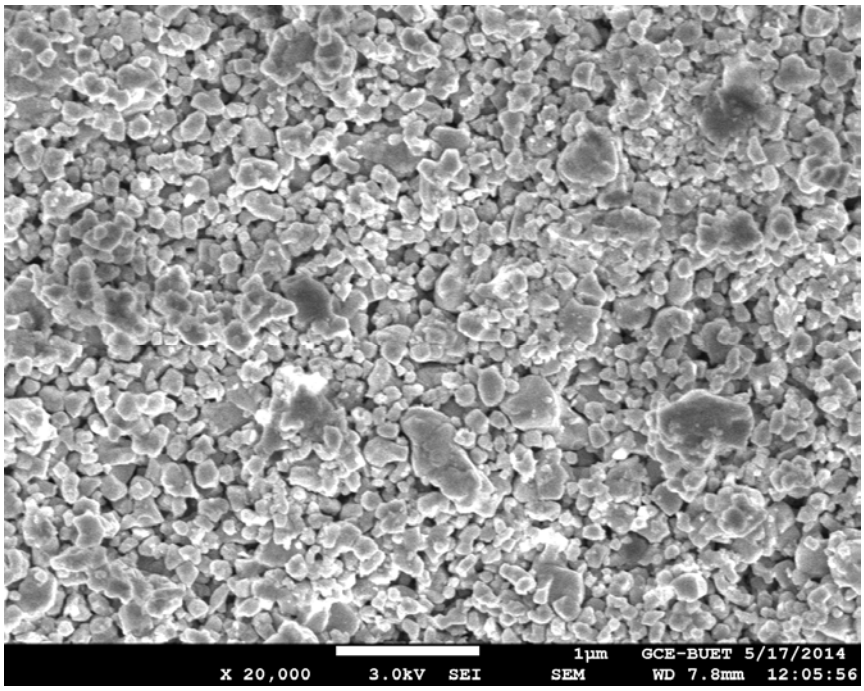

(a)

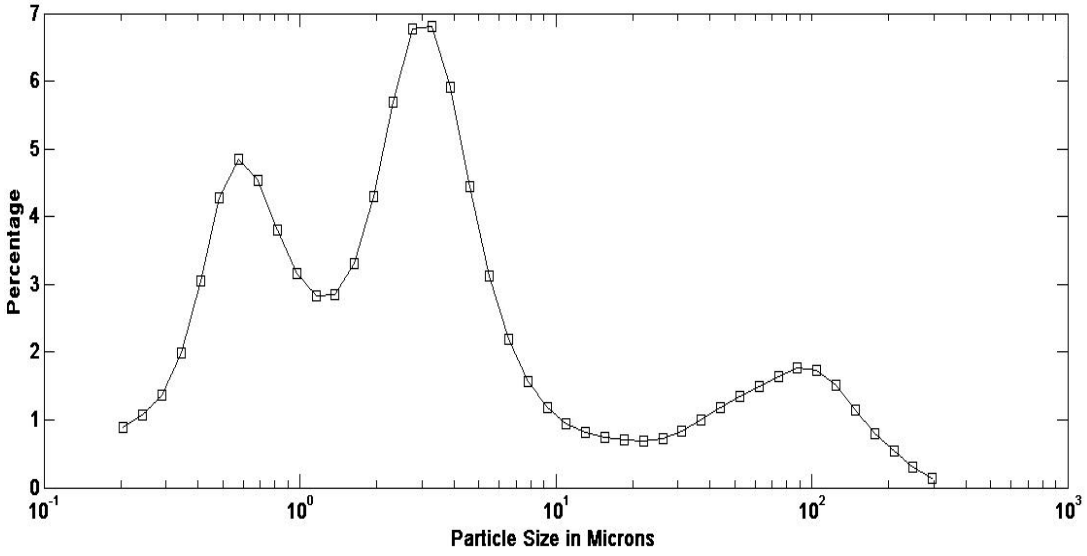

(b)

Figure 4.4 (a) FESEM Micrograph and (b) Corresponding Particle Size Analysis of 1.6 mol% Nb doped Sample

4.2 EDX Study of Calcined Product

EDX study was performed in order to understand the composition homogeneity and diffusion of Nb into product for different doping levels. The EDX data are shown in Figures 4.5-4.10 for different doping level.

Figure 4.6 shows the post calcination EDX peaks of different scanned spots for 0.4 mol% Nb doped $BaTiO_3$ sample, marked in the FESEM image shown in Figure 4.5. The mass percent obtained from the EDX is given in Table 4.1. In point 001 and 002, oxygen, titanium and barium have been found consistent at different positions. Low Nb has been detected by EDX at spot 001 and 002 but no Nb was detected at spot 003. However, EDX peaks representing spot 003 in Figure 4.6-c, confirms the existence of Nb, where the concentration level may be too low to be measured.

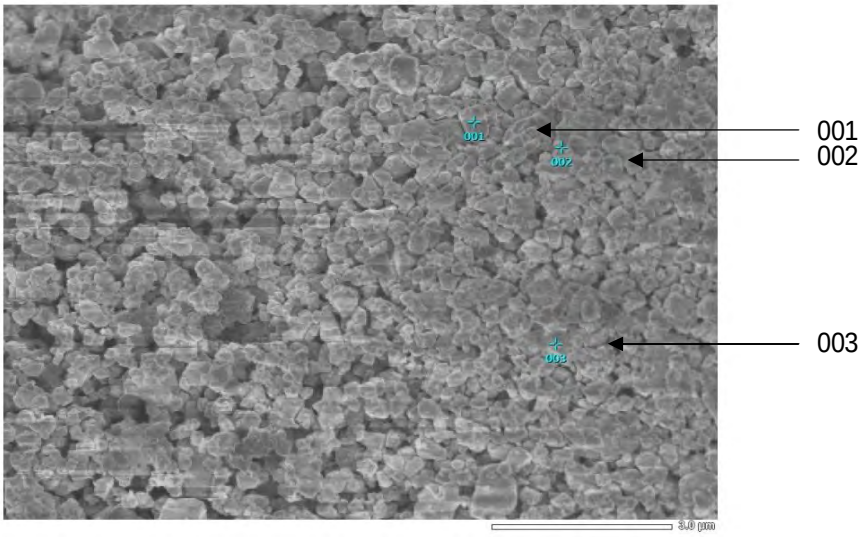

Figure 4.5 FESEM for 0.4 mol% Nb Doped Sample Indicating Points for EDX

Table 4.1 EDX Data for Figure 4.5

Elements	Mass % in Spot 001	Mass % in Spot 002	Mass % in Spot 003
O	30.18	23.69	27.24
Ti	27.46	30.37	29.14
Nb	0.2	0.07	-
Ba	42.15	40.86	43.61

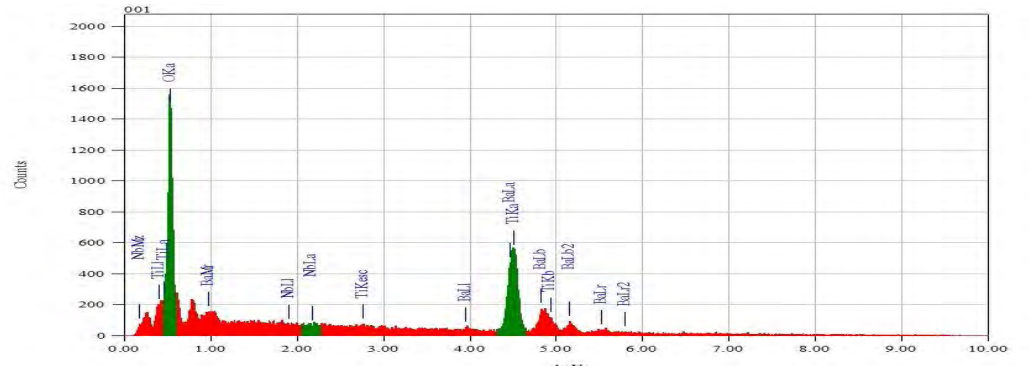

(a)

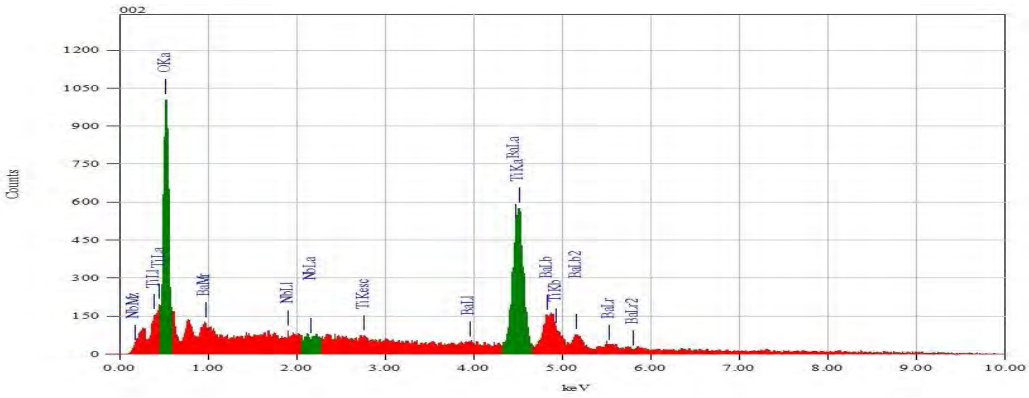

(b)

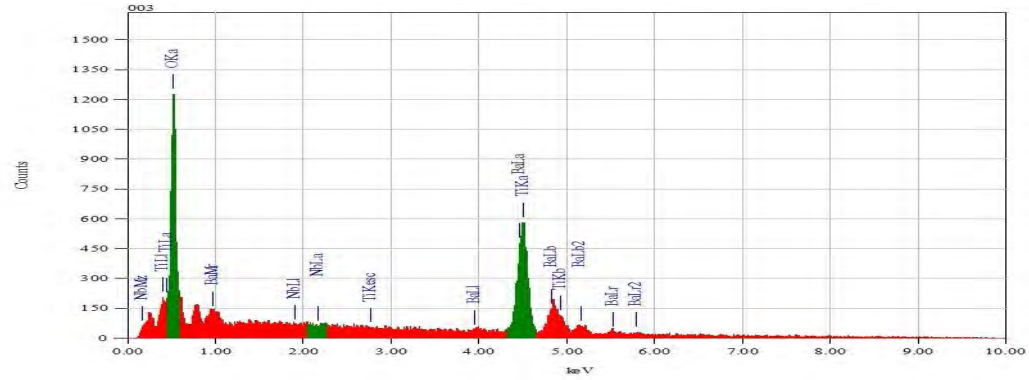

(c)

Figure 4.6 EDX Pattern for Points Shown in Figure 4.5; (a) 001, (b) 002, and (c) 003

For sample doped with 0.8 mol% Nb, inhomogeneous distribution occured not only for Nb, but also for oxygen and titanium as well, as shown in Figures 4.7-4.8 and in Table 4.2. For spot 002 and 003, shown in Figure 4.7, significant variation has been found for oxygen and titanium level, with no Nb detection at all (Table 4.2). However, peaks have been detected for Nb, shown in Figure 4.8(a)-(b) for spot 002 and 003. It is apparently beyond detection limit for those particular spots. Spot 004 has all the components detected (Table 4.2) however, Nb level is low in comparison to the doping level.

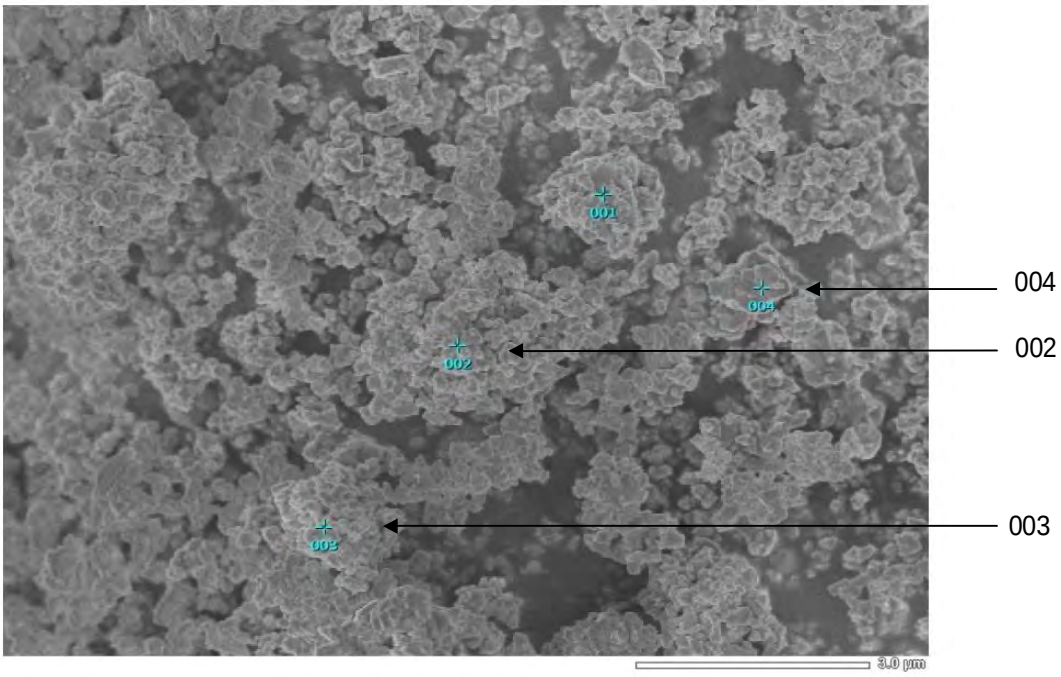

Figure 4.7 FESEM for 0.8 mol% Nb Doped Sample Indicating Points for EDX

Table 4.2 EDX Data for Figure 4.7

Elements	Mass % in Spot 002	Mass % in Spot 003	Mass % in Spot 004
O	40.71	10.07	13.99
Ti	18.96	37.13	32.78
Nb	-	-	0.09
Ba	40.33	52.80	53.13

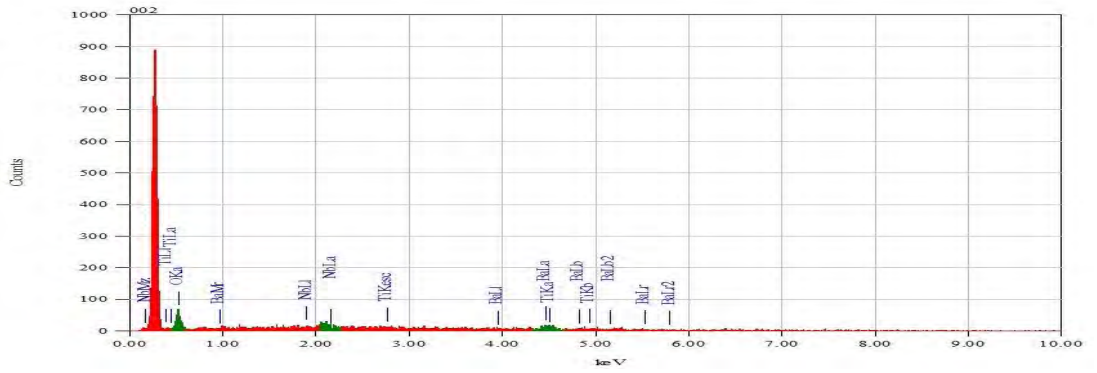

(a)

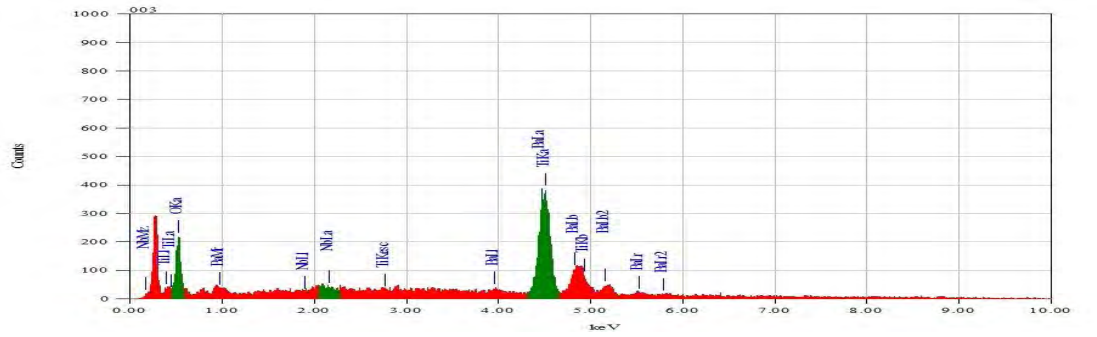

(b)

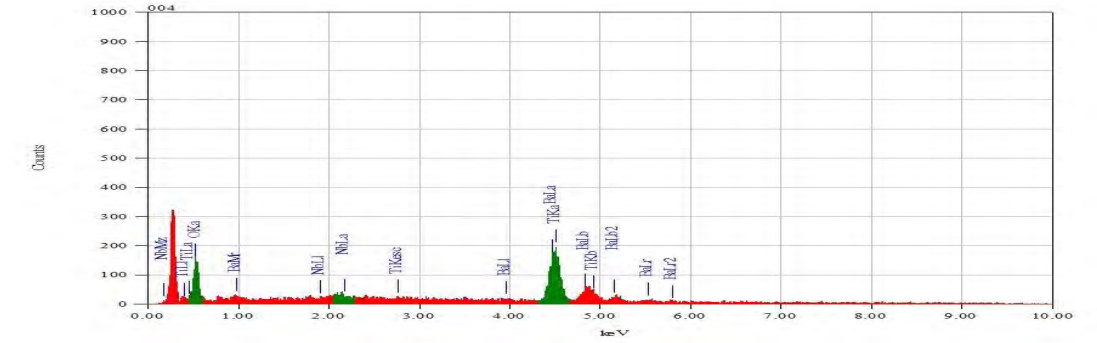

(c)

Figure 4.8 EDX Pattern for Points Shown in Figure 4.7; (a) 002, (b) 003, and (c) 004

Finally, sample doped with 1.6 mol% Nb, higher level of Nb has been detected by EDX (Table 4.3), marked in Figure 4.9 as spot 002, 003 and 004. This was expected as Nb was doped in higher concentrations. Moreover, better homogeneity in Nb distribution was observed in cases of points 003 and 005 in comparison to point 002 (Table 4.3). Though samples were ball milled before and after calcinations, uniform distribution of Nb is still to be achieved. However, it is expected that during sintering the calcined product would obtain further uniformity in distributing Nb throughout the structure. Incorporation of Nb into $BaTiO_3$ has been found very slow, even at very high temperatures and this was reported in early literature as well [35].

Therefore, inhomogeneity was prominent in Nb distribution after calcination for samples doped with 0.4 and 0.8 mol% Nb, whereas better distribution was obtained for 1.6 mol% Nb doped $BaTiO_3$.

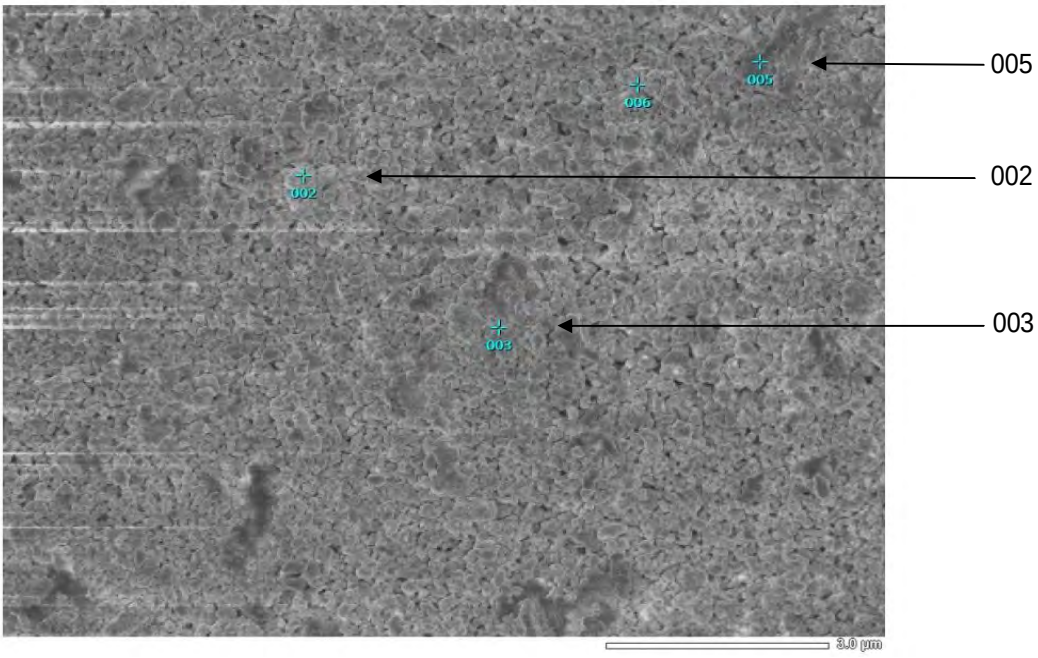

Figure 4.9 FESEM for 1.6 mol% Nb Doped Sample Indicating Points for EDX

Table 4.3 EDX Data for Figure 4.9

Elements	Mass % in Spot 002	Mass % in Spot 003	Mass % in Spot 005
O	24.63	30.29	28.48
Ti	29.78	28.55	27.62
Nb	0.27	1.16	1.26
Ba	45.31	40.00	42.63

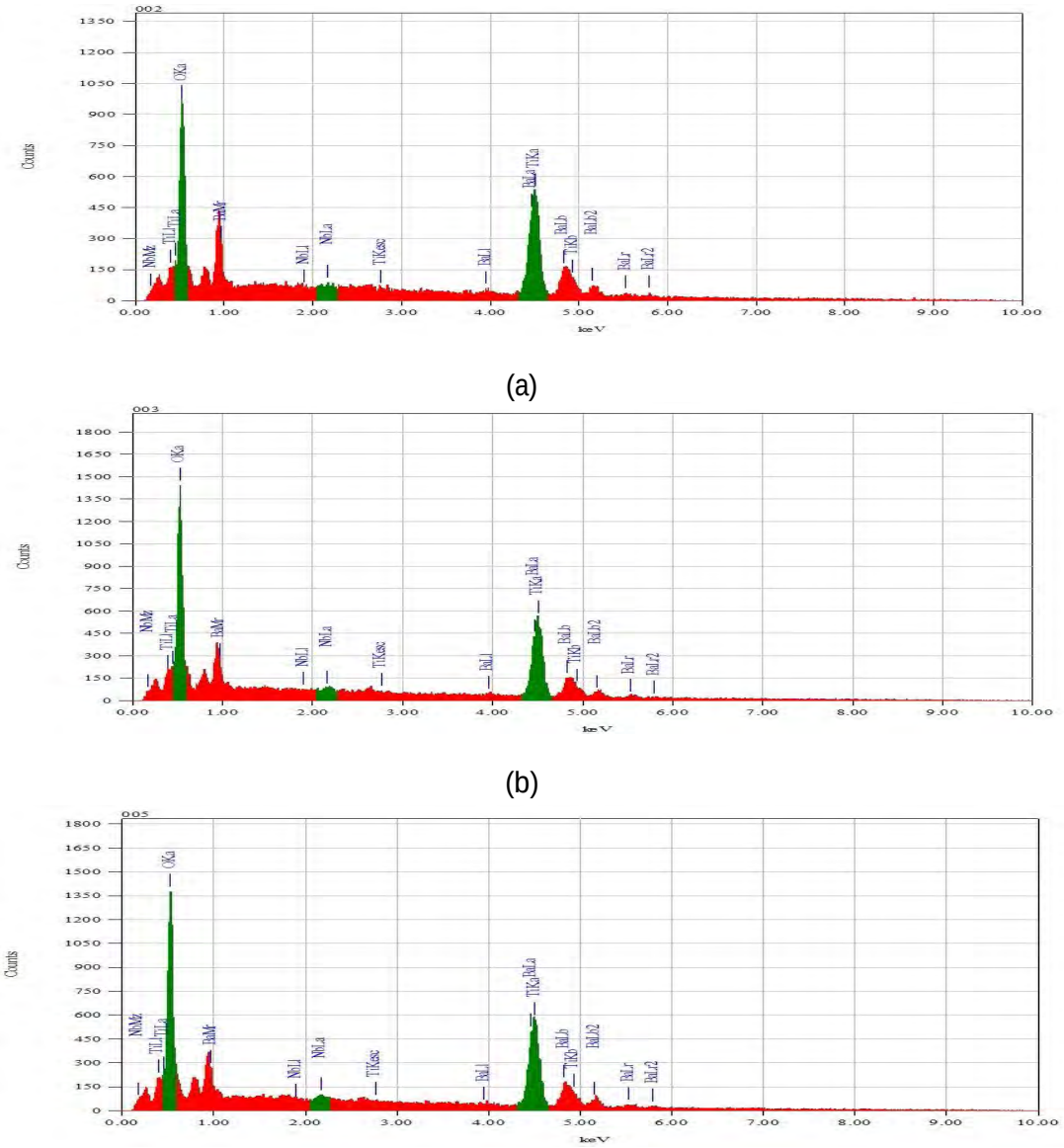

(a)

(b)

(c)

Figure 4.10 EDX Pattern for Points Shown in Figure 4.9; (a) 002, (b) 003, and (c) 005

4.3 X-Ray Diffraction and Phase Analysis

Niobium doped barium titanate was prepared through the process of calcination starting with barium carbonate, titanium dioxide and niobium (v) oxide according to the following reaction.

$$BaCO_3 + (1\text{-}x)\ TiO_2 + x/2\ Nb_2O_5 = (BaTi_{(1-x)}Nb_x)O_3 + CO_2$$

The calcination reaction was conducted at 1300°C. Optimum calcination temperature is important in producing single phase doped barium titanate. Otherwise, raw materials, harmful secondary phases may coexist in considerable amount with

perovskite product, which is evident in the work of Bongkarn *et. al* [23]. Additionally, minimum occurrence of secondary phases or any remnant component from the raw materials must be ensured. At a calcination temperature of 1300°C, both distinct single phase barium titanate and doped barium titante formation have been reported by Manzoor *et. al.* and Bongkarn *et. al.* respectively [20,23]. As both preparations and characterization are involved in this work, making barium titante doped with Nb was one of the major challenges.

After calcination, XRD was carried out on samples for different compositions. The XRD patterns are shown in Figures 4.11 for 0.4 mol% Nb, o.8 mol% Nb and 1.6 mol% Nb respectively.

For 0.4 mol% Nb doped $BaTiO_3$, strong peaks generated from the sample nearly superimposed on the standard position of $BaTiO_3$ indicated by circle. According to Inorganic Crystal Structure Database (ICSD) Collection Code: 86286 and pattern no 01-089-1428, 2θ positions of $BaTiO_3$ within the scanning ranges are 22.170°, 33.512°, 38.868°, 45.229°, 50.924°, 56.165° and 65.789°. From the XRD patterns, successful formation of niobium doped barium titanate was confirmed having perovskite structures. However, peaks from some secondary phases have also been identified in the pattern, for instance the tiny peak nearly at 23.8° just on the right side of the peak of 22.170°. Peaks marked by 'square' symbol corresponds to the phase of $BaNb_{0.5}Ti_{0.5}O_3$ [36] and 'diamond' symbol representing $Ba_6Ti_{14}Nb_2O_{39}$ [27] have also been traced in the patterns. $BaNb_{0.5}Ti_{0.5}O_3$ phase also indicates the replacement of Nb ions into octahedral sites occupied by titanium ions. Since Nb content is very low, the peak heights of secondary phases have been found too low.

0.8 and 1.6 mol% Nb doped $BaTiO_3$ also showed similar pattern in their XRD analysis confirming perovskite $BaTiO_3$ formations with some secondary phases. However, the secondary phase peak on 23.8° as stated earlier has been found diminishing with Nb addition.

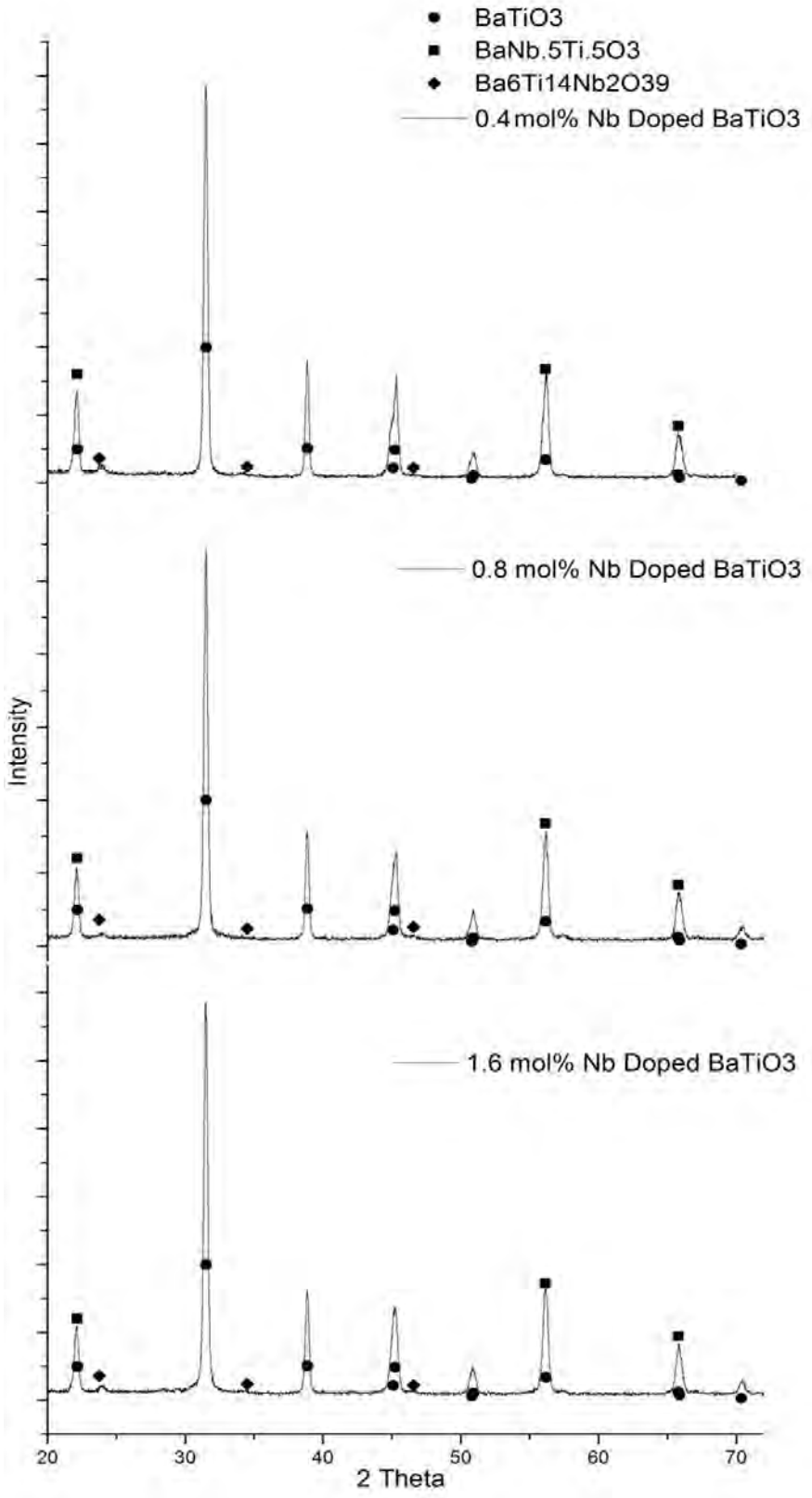

Figure 4.11 XRD Patterns for Samples Doped with 0.4 mol%, 0.8 mol% and 1.6 mol% Nb

Addition of Nb has also significant effects on tetragonality. According to Inorganic Crystal Structure Database (ICSD) Collection Code: 86286 and pattern no 01-089-1428, there are some twin peaks in the pattern of barium titanate because of the tetragonal structure possessed by the same. Twin peak positions corresponding 2θ of 45.104° and 45.229°, representing (002) and (200) planes, have been shown in Figure 4.12 which are substantial in the original XRD peaks shown in Figure 4.11. However, the twin peaks have been found diminishing with Nb doping.

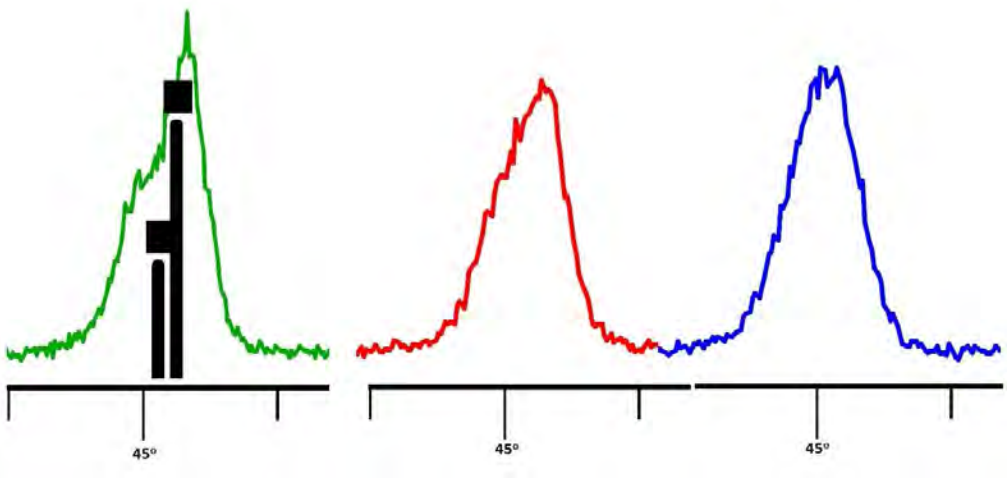

(a) (b) (c)

Figure 4.12 XRD Patterns Showing Decreasing of Tetragonality from Left to Right; (a) 0.4 mol%, (b) 0.8 mol% and (c)1.6 mol% Nb Doped $BaTiO_3$. Solid lines with Squares on Top are Indicating Standard Twin Peak Positions of Pure $BaTiO_3$.

If Lattice parameter along this region of twin peaks of XRD pattern can be calculated and plotted, the variation or diminishing effect of tetragonality with doping of Nb can be visualized further. The lattice parameters, c, a for tetragonal structure calculated from the XRD peaks, shown in Figure 4.12, are tabulated in Table 4.4. The 'a' values increased upto 0.8 mol% Nb doping concentration, and became saturated beyond that level. However, the 'c' values kept reducing with Nb doping. Additionally, a plot of c/a vs doping concentration is shown in Figure 4.13.

Table 4.4 Lattice Parameter for Different Doping Level

Nb Doping Level mol%	C	a
0.4	4.031115	4.00076
0.8	4.017562	4.004108
1.6	4.012505	4.004108

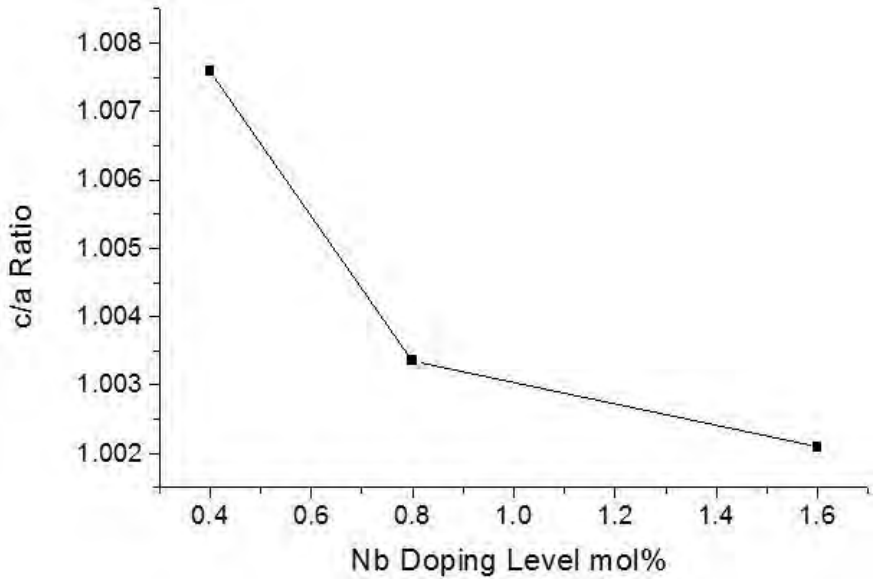

Figure 4.13 Plot Showing Nb Doping Level vs c/a Ratio

From Figure 4.13 it can be said that, with the addition of Nb in barium titanate, tetragonality decreases and from 0.4 mol% to 0.8 mol% doping level, the drop is more drastic. Loosing tetragonality generally stabilizes the cubic phase; thus, reduces the dielectric constant. Bin Cui *et. al.* also showed the loss of tetragonality with Nb addition. In his work, he claimed the shrinkage of host lattice due to Nb addition, caused the lowering of tetragonality [37]. Later on this chapter an attempt will be presented to establish some relationships between this loss of tetragonality and dielectric properties.

Finally, XRD pattern analysis has revealed some remarkable information on successful formation of Nb doped $BaTiO_3$, having perovskite structure along with some secondary phase formations. Moreover, the lowering of secondary phase peak heights and drop of tetragonality with Nb doping has also been identified.

4.4 XRF Study

After calcination and required processing, samples were sintered at a range of 1350-1550°C. XRF analysis of the samples was performed and the obtained data is shown in

Table 4.5 being compared with original calculated data or amount of sample added at the beginning of experiment. Sample containing 0.4 mol% Nb was checked by XRF which was sintered at 1475°C. 72.1293 % of $BaCO_3$, 28.679 % of TiO_2 and 0.19166 % of Nb_2O_5 were added initially and the final sintered product provided 61.9858% BaO, 36.874% TiO_2 and 0.2576% NbO after XRF analysis. Furthermore, calculated weight percentage after sintering is also shown in Table 4.5.

Table 4.5 XRF Data Compared with Calculated Weight Percent

Calculated Weight Percent Initially Added	**Weight Percent Calculated After Sintering**	**Weight Percent Measured After Sintering by XRF**
$BaCO_3$ 72.1293 %	BaO 66.0098%	BaO 61.9858 %
TiO_2 28.679 %	TiO_2 33.67%	TiO_2 36.874 %
Nb_2O_5 0.19166 %	NbO 0.225%	NbO 0.2576 %

A good consistency of mixed or calculated materials was found with recovered materials after sintering. From the XRF data, change of concentration was found for each of the components. This may occur due to the calcination reaction, where barium carbonate decomposes and emission of carbon-di-oxide occurs. As a result, change in percentage of components occurred. Moreover, calculated and measured data after sintering showed slight variations and this may be attributed to the adsorption of moisture in sample. Additionally, using no certified reference material during this scan may also produce this variation.

So, after a long processing from raw powders to sintered mass via calciantion, overall recovery of materials was obtained satisfactory.

4.5 Optimizing Sintering Parameters

After processing, calcined powders were pressed and sintered at different sintering temperatures. Optimum sintering temperature along with, other sintering parameters, depend on the composition of materials. Sintering parameters optimized for one particular composition, may not be appropriate for other compositions. So, optimum sintering temperatures can be obtained by trial and error method, and for different compositions, optimum sintering temperatures may be different [38].

In this work, sintering parameters were optimized initially with sample doped with 0.4 mol% Nb. Further works, were then accomplished for different doping levels around the optimized parameters. Initially, samples containing 0.4 mol% Nb were sintered at a range starting from 1350°C to 1550°C. After sintering, densities of the samples were measured. The density variations with sintering temperatures are plotted in Figure

4.14. Low density resulted from the sample sintered at 1300℃ however, with increasing sintering temperature density increased upto 1450℃ or a slightly above it. Then, a decreasing trend was found. Low firing temperature may result incomplete densification, thus low density whereas, high firing temperature may produce coarse grain with trapped pore inside, also causes low density.

Similar trend can be found for percent theoretical density achieved, which is plotted in Figure 4.15. On the basis of density data, it can be said that maximum density occurred for sample fired at 1450°C. Therefore, for sample doped with 0.4 mo% Nb, optimum sintering temperature is 1450°C however, in order to get conclusive decision, microstructure and dielectric properties such as dielectric constant variations along with sintering temperature, would be very useful.

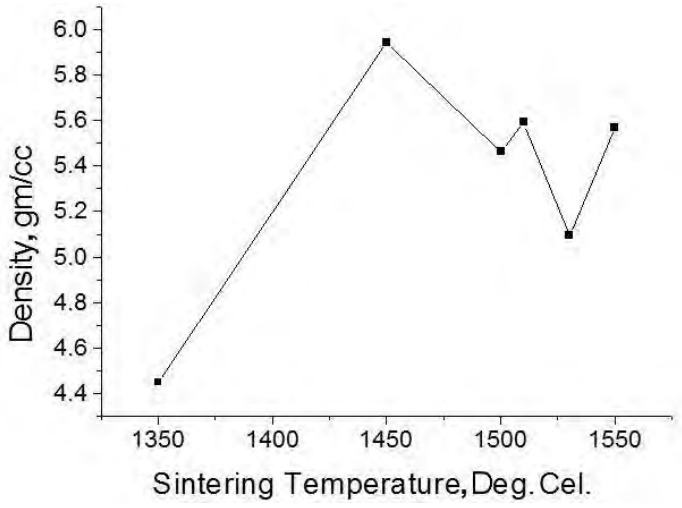

Figure 4.14 Density Variations with Sintering Temperature

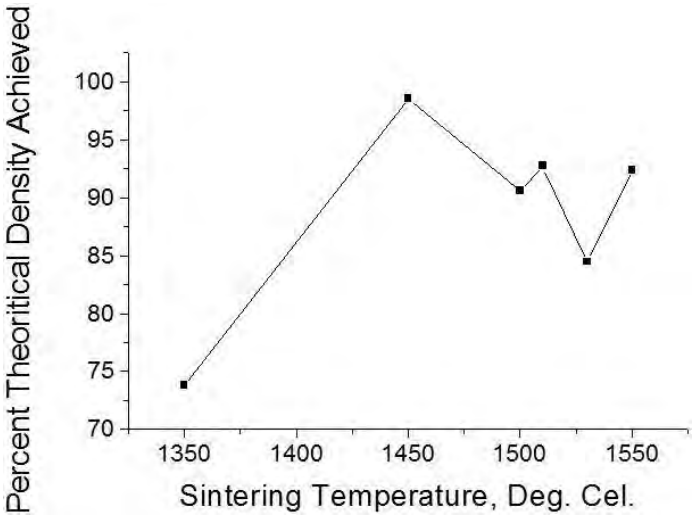

Figure 4.15 Percent Theoretical Density Variations with Sintering Temperature

If samples doped with 0.4 mol% Nb are analyzed and their dielectric constant k for different frequencies can be plotted against the samples' sintering temperature, a clear indication regarding optimum sintering temperature can be obtained. Such plot is shown in Figure 4.16.

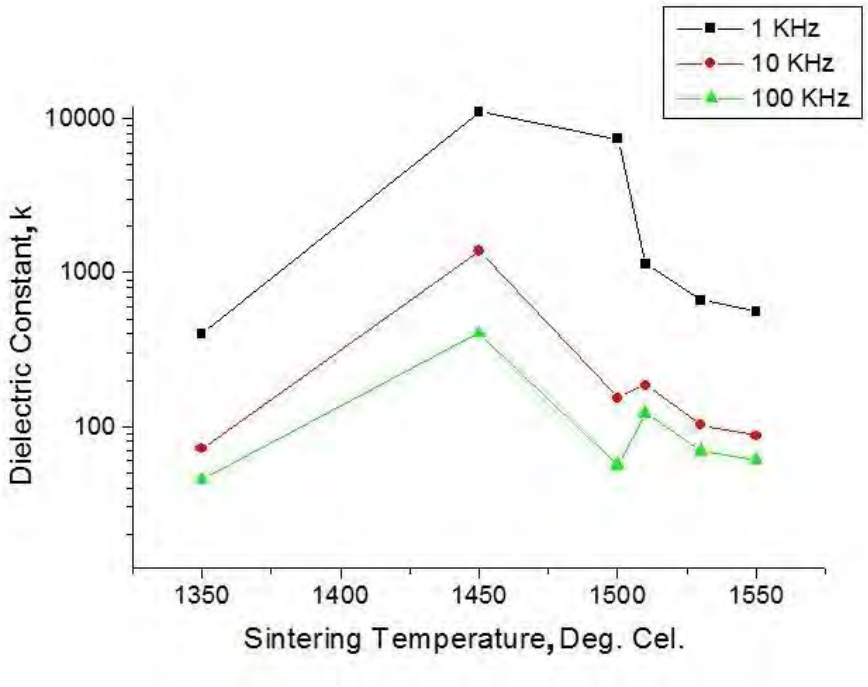

Figure 4.16 Curve Showing k Values against Samples' Sintering Temperature with Different Applied Frequencies Doped with 0.4mol% Nb

From Figure 4.16 a similar trend can be seen with density and percent theoretical density as shown in Figures 4.14 and 4.15. Minimum value of k resulted for sample sintered at 1350°C. Maximum value of dielectric constant k was found for sample sintered at 1450°C. However, above that sintering temperature, k values dropped slightly. Therefore, again sintering temperature of 1450°C was found optimum for 0.4 mol% Nb doped $BaTiO_3$.

For frequency dependency, a drop of k values was observed with increasing frequencies from 1 KHz to 100 KHz in Figure 4.16. This may occur due to the freezing of polarization mechanisms with increasing frequencies which are namely electronic, ionic, dipolar and interfacial [7], already explained in section 2.5. However, drastic drop of k values with increasing frequencies is not clear.

From SEM micrographs shown in Figure 4.17 it can be said that, $BaTiO_3$ doped with 0.4 mol% Nb had their grain size increased with increasing sintering temperatures. Furthermore, trapped pore inside grain has also been identified and marked in the micrograph.

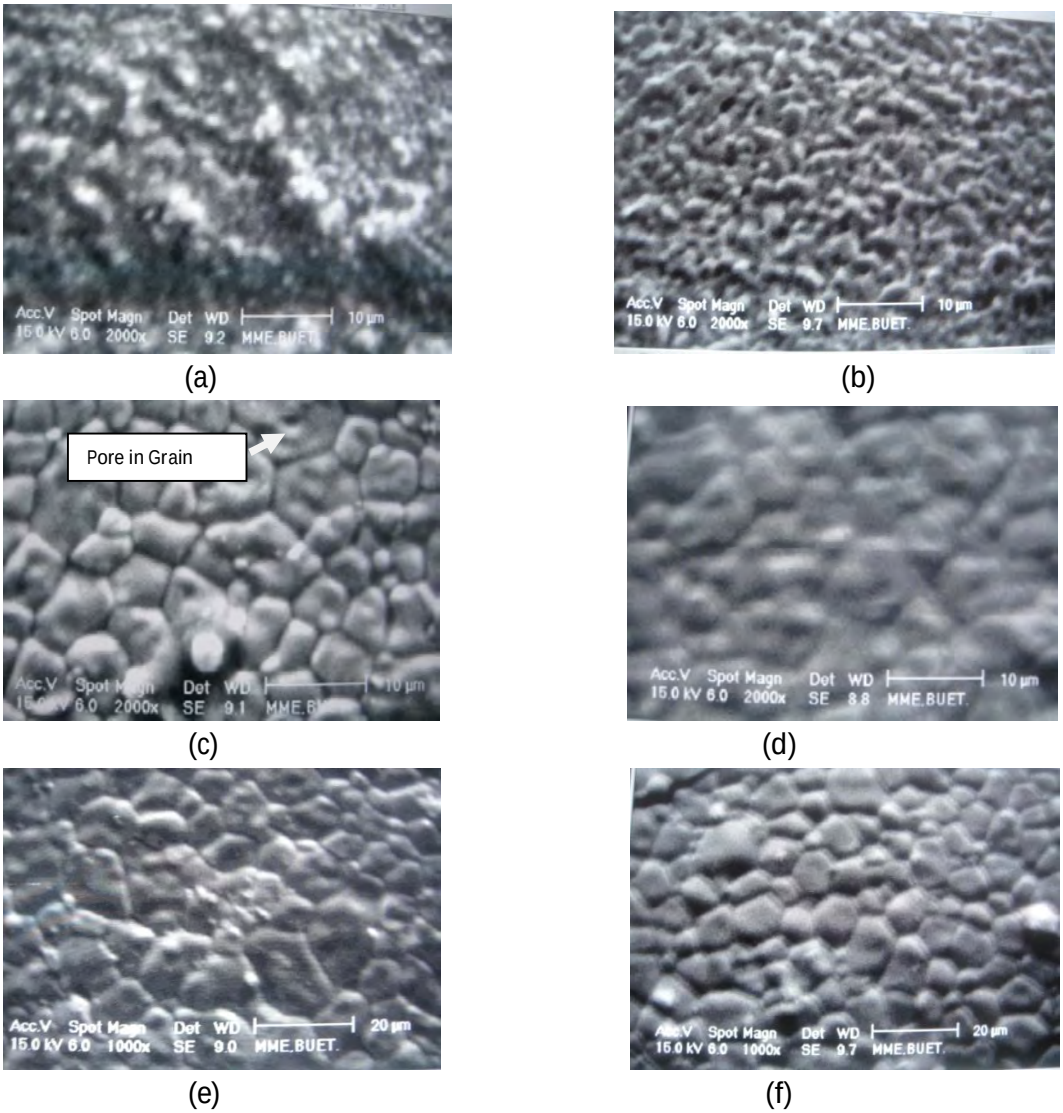

Figure 4.17 Microstructures of 0.4mol% Doped Samples at Different Sintering Temperatures (a) 1350°C (b) 1450°C (c) 1500°C (d) 1510°C (e) 1530°C (f) 1550°C

From Figures 4.14-4.17, it can be concluded that, increasing sintering temperature from 1350°C to 1450°C for $BaTiO_3$ doped with 0.4 mol% Nb, showed increased density having fine grain size resulting good dielectric constant values upto 1450°C. However, beyond 1450°C density values dropped upto 1550°C and the reason behind this may be the coarse grain and trapped pore inside the grain as indicated in Figure 4.17. In accordance with the lowering of density values, grain size increased with increased sintering temperatures. Finally, drop of dielectric constant is quite consistent with the other result as coarse grain, low density material always have lower dielectric constant values.

Other sintering parameters, such as soaking time during sintering and heating rate, were also optimized by trial and error method on different properties, keeping the composition fixed.

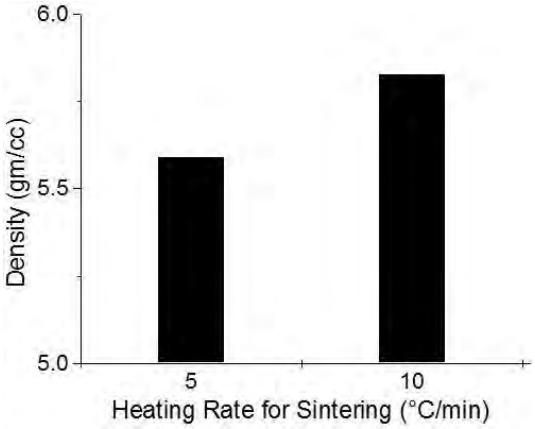

(a)

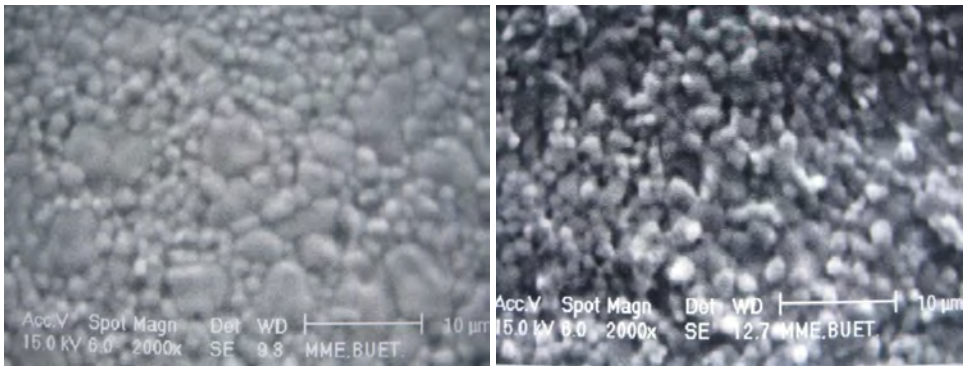

(b) (c)

Figure 4.18 (a) Plot Showing Density Variations with Heating Rate, (b) SEM Micrographs of the Samples with Heating Rate of 5°C/min (c) 10 °C/min

Effects of heating rate on density and microstructures have been investigated for sample containing 0.4 mol% Nb, being sintered at 1475°C in order to get optimum heating rate. Slower heating can result in coarse grains, which in turn, reduces dielectric constant as explained in Section 2.13. On the other hand, faster heating may inhibit grain growth [39], which is good for dielectric properties. Therefore, heating rate should be optimized in such a way that a fine grained microstructure with high density can result. From Figure 4.18(a), it can be seen that, heating rate of 10 °C/min resulted higher density than a heating rate of 5°C/min. This may happen due to the formations of bimodal grain in the microstructure with a heating rate of 5°C/min as shown in Figure 4.18(b) where coarse grain with some porosities are evident. On the other hand, homogenous and fine grain-microstructure has been observed for the sample with a heating rate of 10 °C/min (Figure 4.18(c)).

For finding optimum soaking period during sintering, soaking period for $BaTiO_3$ doped with 0.4 mo% Nb, was varied from 0 hour to 2 hour, during firing at 1450°C. Prolong heating may result in formation of coarse grain which may trap pores inside and can result poor dielectric properties. On the other hand, very short soaking may result incomplete densification. So, soaking period should be optimized in order to get fine grained material that can result high dielectric constant.

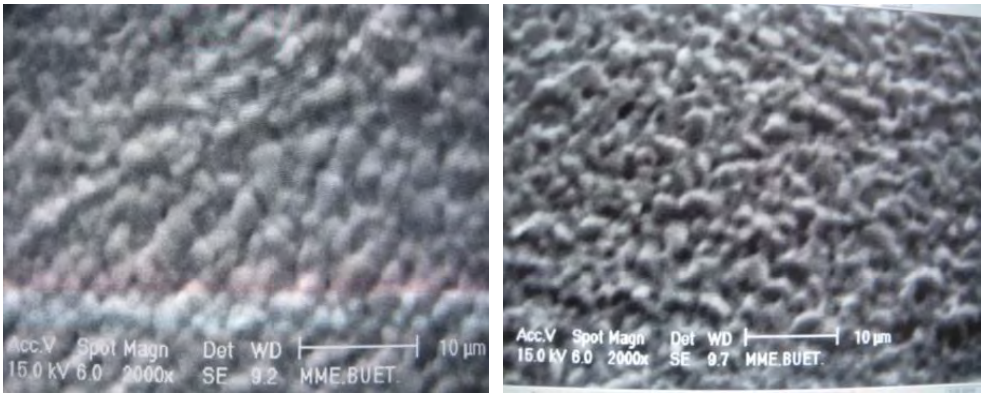

(a) (b)

(c)

Figure 4.19 Effect of Soaking Period on Microstructure with Soaking Time of (a) 2 hours, (b) 1 Hour, (c) O hours

From the micrographs shown in Figure 4.19, it is evident that increased grain size resulted with increased soaking hour when samples were sintered at 1450°C doped with 0.4 mol% Nb. This also has tremendous effect on dielectric constant values as shown in Figure 4.20. At different applied frequencies, same result was obtained with a lowering of k values with lowering of soaking time. Therefore, 2 hours of soaking was found optimum and other experiments were also conducted by soaking the samples for 2 hours at sintering temperature.

Overall, for 0.4 mol% Nb doped $BaTiO_3$, 1450°C of sintering temperature with a heating rate of 10°C/minute and soaking period of 2 hours were found optimum in response to the density, microstructures and dielectric behaviors.

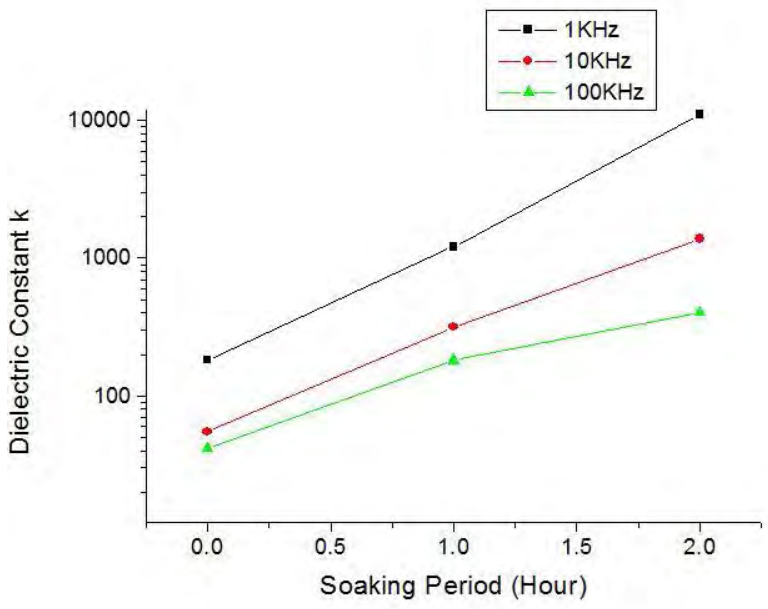

Figure 4.20 Dielectric Constant k, for Different Soaking Period for 0.4 mol% Nb doped $BaTiO_3$ being Sintered at 1450°C

4.6 Effect of Nb Doping on Curie Temperature

Variation of dielectric constant (k) values with temperature was investigated at an applied frequency of 0.1 KHz for sample containing 0.4 mol% Nb sintered at 1450°C as shown in Figure 4.21. From Figure 4.21, it is evident that, because of the doping of Nb into $BaTiO_3$, Curie temperature of the sample shifted towards lower side. Generally, for pure $BaTiO_3$, the Curie temperature is 120°C. A characteristic tetragonal to cubic phase transition was detected at a temperature near 100 or 110°C where ferroelectric to paraelectric transition occurred indicated by the abrupt drop of k values [26].

The effect of Nb doping into $BaTiO_3$ in shifting the Curie temperature or phase transition temperature has been a controversial issue [4]. As the Curie temperature of $BaTiO_3$ is generally 120°C, both increase and decrease of Curie temperature due to the addition of Nb were reported in different literatures [26, 27, 4].

In this case, lowering of Curie temperature has been detected due to Nb addition. It is believed that, less thermal energy is required to break the asymmetric balance of Nb-O bond, compared to Ti-O bond, which in turn, results in lowering the Curie temperature with the increase in Nb content [4].

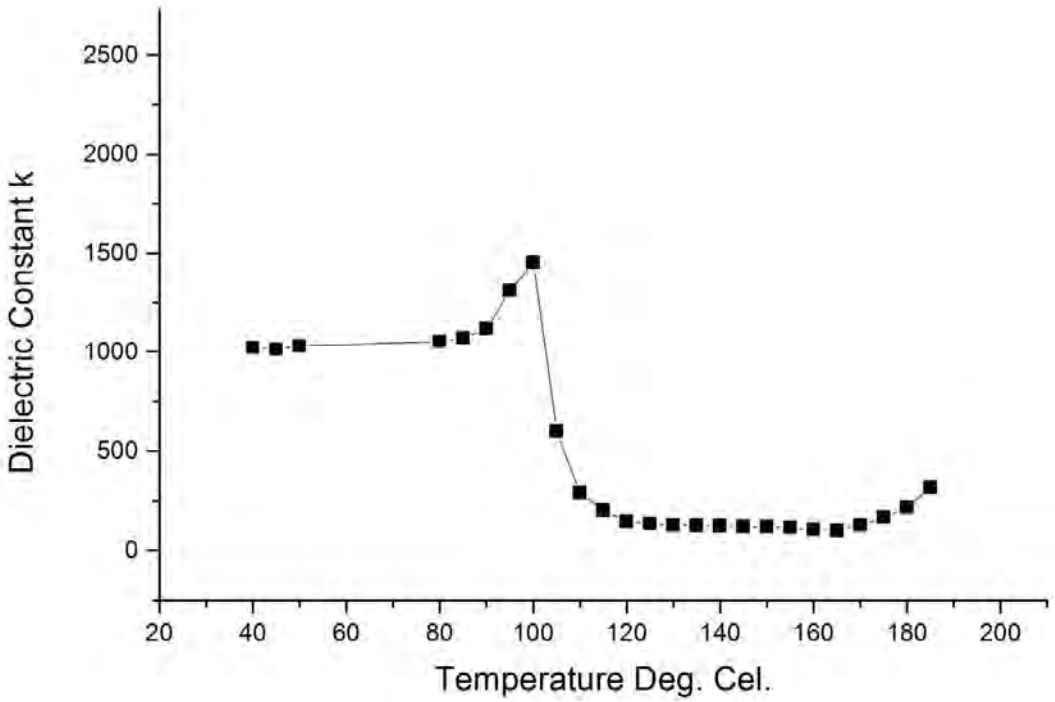

Figure 4.21 Dielectric Constant k, as a Function of Temperature

4.7 ANOVA Modeling

Analysis of variance (ANOVA) modeling was performed in order to obtain the significance of variables on properties. Different sets of experiments were required to perform ANOVA. SEM micrographs with a brief list of the experiments with associate properties have been shown in Table 4.6 and in Figure 4.22.

Table 4.6 Samples' Associated Properties with Different Sintering Temperatures

Nb, mol%	Sintering Temperature, °C	Average Grain Size, µm	Density, gm/cc
0.4	1475	1.975	5.829
0.8	1475	1.232	6.0298
1.6	1475	1.235	5.8407
0.4	1450	1.638	5.91
0.8	1450	1.206	5.677
1.6	1450	0.90725	5.518
0.4	1425	1.975	5.96
0.8	1425	1.30875	5.99
1.6	1425	1.045	5.51

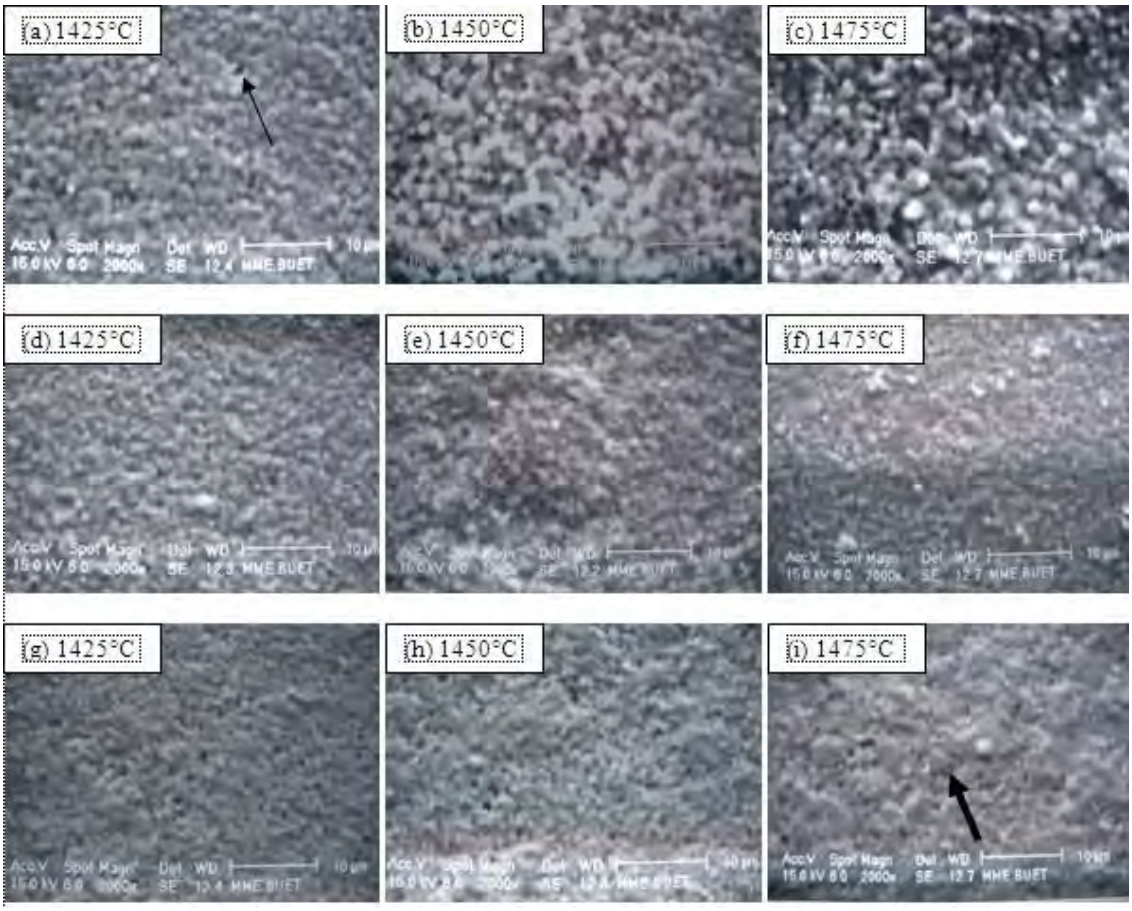

Figure 4.22 SEM Micrograph of $BaTi_{1-x}Nb_xO_3$ Samples with Different Sintering Temperature and Doping level (a, b, c) 0.4 mol% Nb, (d, e, f) 0.8 mol% Nb and (g, h, i) 1.6 mol% Nb. Arrows Indicating in Figure 4.22-a and 4.22-i Porosity and Coarse Grain Respectively

Following the procedure mentioned in Section 3.3.8, ANOVA modeling was performed on different parameters for different sets of experiments. Pareto charts were also made in order to project the variables' significance on particular properties.

The first Pareto chart was developed for different Nb concentration taking as variable 'A' and different sintering temperature as variable 'B' and their significance on density measured in gm/cc, Figure 4.23. The corresponding data set is given in Table 4.7. From Figure 4.23, it can be said that, sintering temperature has much more stronger effects on sample density than the combined effect of both temperature and Nb concentration. Moreover, the effect of Nb concentration alone on density has been found least than the others. It is the column with larger value in Pareto charts, that has more significance than the others. In addition to that, Δ/2 values from Table 4.7, calculated as explined in Section 3.3.8, indicate that, all the Δ/2 values are negetive for 'A', 'B' and 'AB'. This simply states that, increasing Nb content as well sintering temperature individually or combinedly will reduce the density of Nb doped $BaTiO_3$

within the mentioned temperature range. Higher sintering temperaure may cause the entrapment of pores inside the grain during faster grain growth thus reducing density.

Moreover, increasing Nb content may produce microstructure associated with porosity which may be another reason for reducing density and this type of phenomena has also been reported earlier [27].

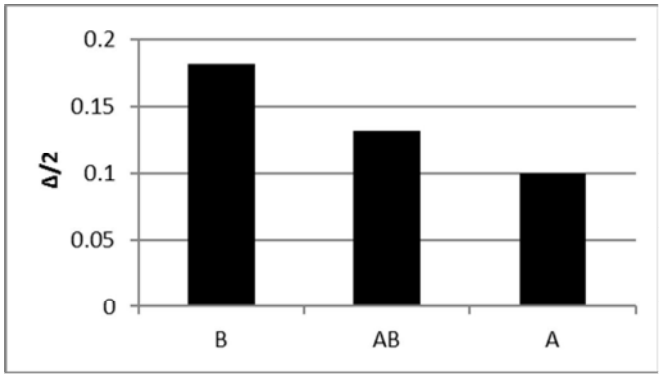

Figure 4.23 Pareto Chart for Density; A=Nb Concentration in mol%, B=Sintering Temperature °C

Table 4.7 Pareto Chart Data for Density

Run	Nb mol% (A)	Temperature °C (B)	A	B	AB
1	0.4	1425	-	-	+
2	0.4	1450	-	+	-
3	0.8	1425	+	-	-
4	0.8	1450	+	+	+
		Δ/2	-0.1	-0.1815	-0.1315

The next modeling was executed in order to identify the significance of Nb concentration 'C' and sintering temperature 'D' on grain size, measured in µm of the sintered samples. From the Pareto chart, it is evident that Nb concentration has stronger effect on grain size than sintering temperature in region of 1425-1450°C, whereas combined effect of 'C' and 'D' has been found minimum in this case (Figure 4.24). From the Δ/2 values of Table 4.8, it can be said that negetive value of 'C' reduces grain size with increasing Nb content which has also been reported in [4, 40], whereas positive value of 'D' or sintering temperature increases grain size which is common phenomena and reported in early literatures [41]. Increasing both 'C' and 'D' simultanously reduces grain size as 'CD' has negetive Δ/2 . From the microstrctures of the sintered sample a better interpretation of this modeling can be made (Figure 4.22).

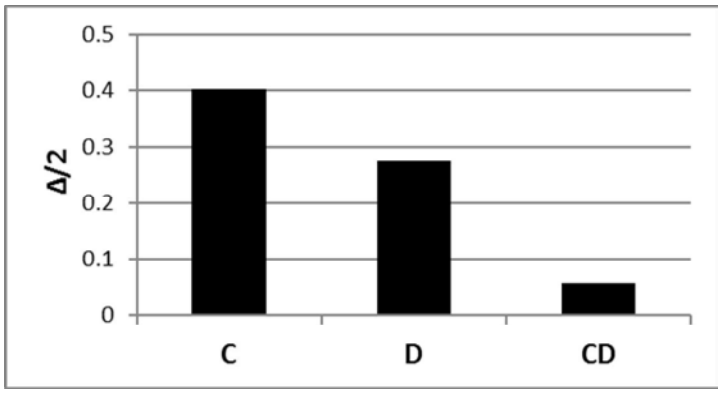

Figure 4.24 Pareto Chart for Grain Size; C=Nb Concentration in mol%, D=Sintering Temperature °C

Table 4.8 Pareto Chart Data for Grain Size

Run	%Nb (C)	Temperature °C (D)	C	D	CD
1	0.4	1425	-	-	+
2	0.4	1450	-	+	-
3	0.8	1425	+	-	-
4	0.8	1450	+	+	+
		Δ/2	-0.4025	0.2758333	-0.0575

The final pareto chart was developed considering holding time during sintering 'E' and applied frequency to the sintered product as 'F' to understand their significance on dielectric constant (Figure 4.25). Samples containing 0.4 mol% Nb, sintered at 1450°C were taken for this analysis. It is the applied frequency, that strongly affects the dielectric constant values than the others.

From Table 4.9, it is evident that, Δ/2 value is positive for 'E'. This indicates that, sufficient time must given to the samples during sintering in order to increase the dielectric constant of the material. As porosity in materials can lower the dielectric constant, sufficient soaking time is required to remove those pores. However, excessive soaking can increase grain size which can be detrimental for dielectric properties. On the other hand, Δ/2 values for 'F' or frequency is found negetive, which indicates that, increasing frequency will reduce the dielectric constant of the material. This occurs as, the mechanisms of polarization in dielectric materials; electronic, ionic, interfacial and dipolar start to deactivate with increasing frequencies [7].

Overall, sintering temperature, Nb concentrations and applied frequency have been identified significant for the properties of density, grain size and dielectric constant respectively.

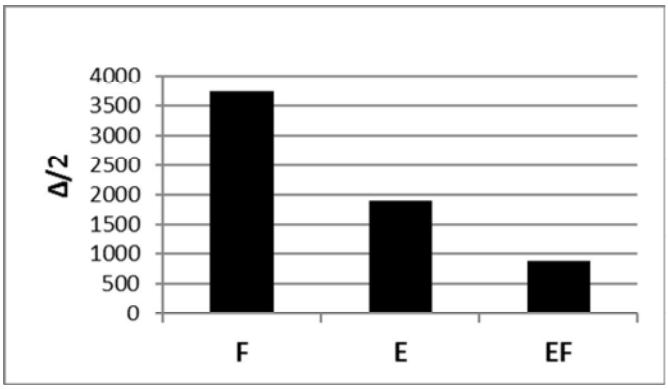

Figure 4.25 Pareto Chart for Dielectric Constant k; E=Holding Time in Hour, F=Applied Frequency in KHz

Table 4.9 Pareto chart data for dielectric constant.

Run	Holding hr (E)	Frequency kHz (F)	E	F	EF
1	0	0.1	-	-	+
2	0	1	-	+	-
3	1	0.1	+	-	-
4	1	1	+	+	+
		Δ/2	1908.6	-3739.09	-874.83

4.8 Effects of Nb Doping on Different Properties

Finally, $BaTiO_3$ samples doped with 0.4 mol% Nb, 0.8 mol% Nb and 1.6 mol% were studied altogether and doping effects on different properties such as density, grain size, and dielectric constant and dielectric loss have been investigated. Correlation of these has also been made with microstructures observed by FESEM.

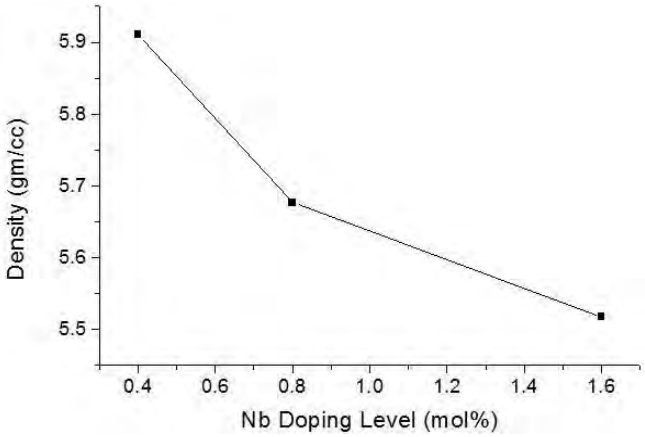

Figure 4.26 Density Variations with Nb Doping Level

In Figure 4.26, effect of doping level on density is plotted for samples sintered at 1450°C. As explained earlier in Section 4.5, optimum sintering temperature depends

on composition of materials, and Figure 4.26 has projected that. Lowering of density occurred with Nb addition, where samples' sintering temperature kept constant at 1450°C. Sintering temperature which has been optimized for 0.4 mol% Nb doped $BaTiO_3$, may not be optimum for 0.8 and 1.6 mol% doped $BaTiO_3$. In Figure 4.27, theoretical densities has also followed similar trend with density data as shown in Figure 4.26.

Incomplete removal of pore or trapped pore in the grains is one of the main reasons for lowering density as well as obtained theoretical density. In this scenario, addition of Nb may have promoted the porosity issue in lowering density which will be explained in the microstructure study of the later part of this section.

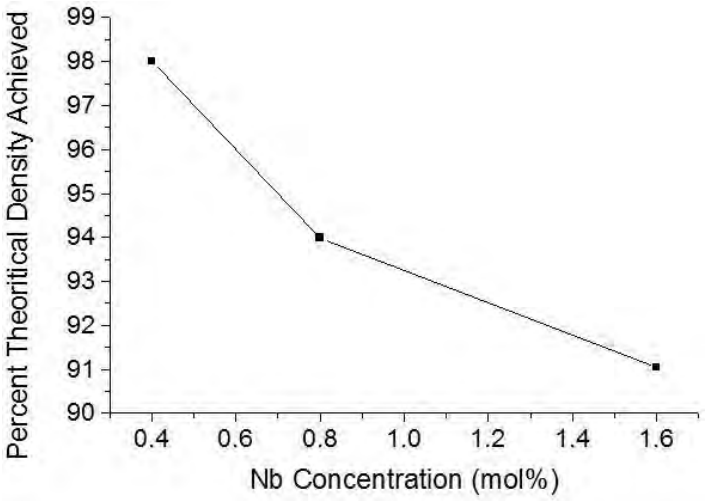

Figure 4.27 Percent Theoretical Density Variations with Nb Doping Level

Effect on dielectric constant (k) due to Nb addition is plotted in Figure 4.28 with different applied frequencies for samples sintered at 1450°C. As increasing frequencies make the polarization mechanisms deactivated, which has already been explained earlier in Section 2.5, curves showing lower k values with increasing frequencies, have been observed for different doping level. For 0.4 and 0.8 mol% Nb concentration, the fall of k values are very drastic than for 1.6 mol% Nb sample.

In addition, with the increase of Nb concentration, the k values at all frequencies have been found to decrease. However, the values are too low for high Nb content. Increase of Nb can reduce the dielectric constant of materials and this was also reported earlier [4]. The low values can be explained by the work of N. Maso *et.al.* [42], where k values below 500 have been reported at room temperature with an applied frequency of 50Hz. Similar type of result was also reported by Stojanovic *et. al*. [43]. Therefore, both Nb and frequency have played role simultaneously to reduce the k values of the samples. Further investigation on this has been made in the later part of this section.

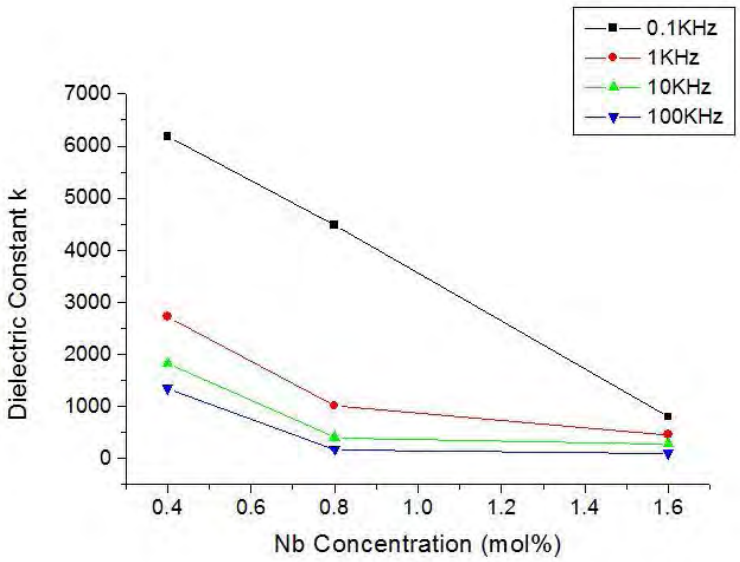

Figure 4.28 Dielectric Constant Variations with Different Doping Level

Dielectric loss has to be as low as possible in order to get better polarizations with applied frequency. Minimum loss was observed at 0.1 KHz for sample doped with 0.4 mol% Nb, being sintered at 1450°C (Figure 4.29). However, rise of dielectric loss was observed with the increase of Nb content. Lowering of dielectric constant may be attributed to this rise of loss which has been found consistent with Figure 4.28.

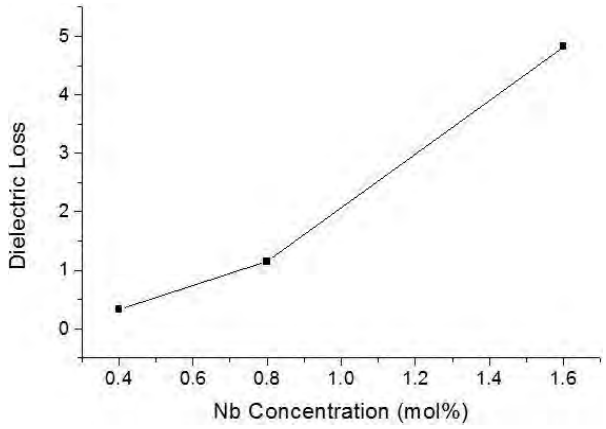

Figure 4.29 Dielectric Loss as Function of Nb Concentration

In Figure 4.30, the FESEM images of samples with each doping level, being sintered at 1450°C, are shown. Lowering of grain size occurred with Nb addition. Furthermore, remarkable amount of porosities are evident for 1.6 mol% doping concentration. As a result, it can be said that Nb inhibits grain growth when added with $BaTiO_3$. This was also reported in early works as well [4]. Effect Nb addition on average grain size is plotted in Figure 4.31. By image analysis, the grain number per unit area has also been calculated. 0.798 grain per μm^2, 1.0789 grain per μm^2 and 20.956 grain per μm^2 have

been calculated for 0.4 mol% Nb, 0.8 mol% Nb and 1.6 mol% Nb doped $BaTiO_3$ respectively. This was found consistent with grain size reduction with Nb addition.

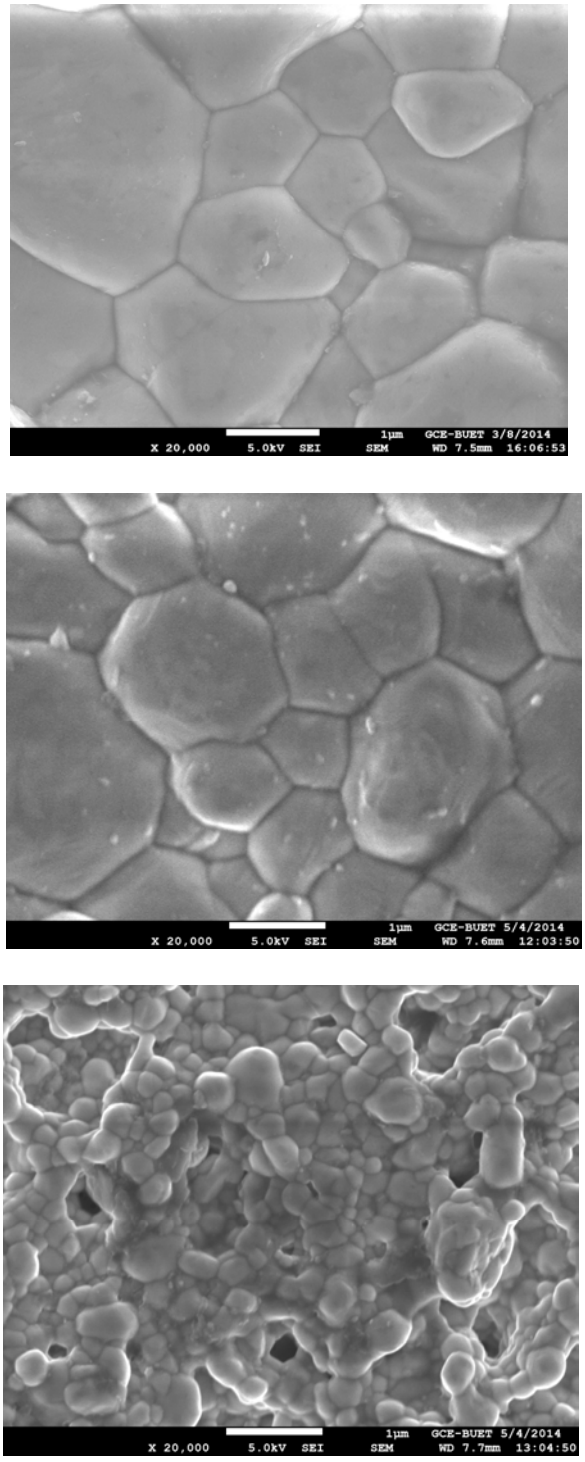

(a)

(b)

(c)

Figure 4.30 FESEM Images of (a) 0.4mol% Nb, (b) 0.8 mol% Nb and (c) 1.6 mol% Nb Doped $BaTiO_3$ Sintered at 1450°C

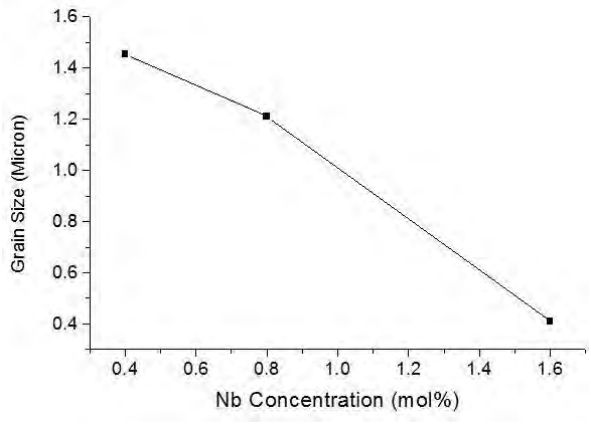

Figure 4.31 Grain Size Lowering with Nb Addition

Though finer grain size was obtained with Nb addition, porosities were evident especially for 1.6 mol% Nb doped barium titanate (Figure 4.30-(c)). Average size of the porosities was measured as 0.288 μm. Porosity size was measured by using Image J software package, where sizes of different porosities were measured and average value was taken. From Figures 4.26-4.31 it can be concluded that, Nb has grain refinement ability however, with the addition of Nb dielectric constant value dropped with a large margin. Generally, coarse-grained barium titanate has lower dielectric constant than fine- grained barium titanate at room temperature. However, it is believed that, when grain size of barium titanate is below 700 nm or 0.7 μm, the structure of $BaTiO_3$ changes from tetragonal to pseudocubic and dielectric constant becomes very low. For doped condition, situation becomes more complex as there is influence of dopant in phase transition, structure and properties [43]. In Figure 4.30-c, 1.6 mol% Nb doped $BaTiO_3$ has an average grain size below 0.6 μm with some pores. As a result very poor dielectric constant resulted from this sample. Therefore, 1450°C may not be the optimum sintering temperature for this doping level with a soaking time of 2 hours. Prolonged soaking or higher sintering temperature may raise the grain size and remove those pores. That will be favorable for getting better dielectric properties. Moreover, loosing tetragonaity, as reported in Figure 4.12, with Nb addition may also contribute to the loss of dielectric constant. For this reason, sample doped with 1.6 mol% Nb was sintered slightly at higher temperature; 1475°C and corresponding dielectric constant was measured and plotted with that of the sample of same composition being sintered at 1450°C. The plot is shown in Figure 4.32 in association with the FESEM micrographs.

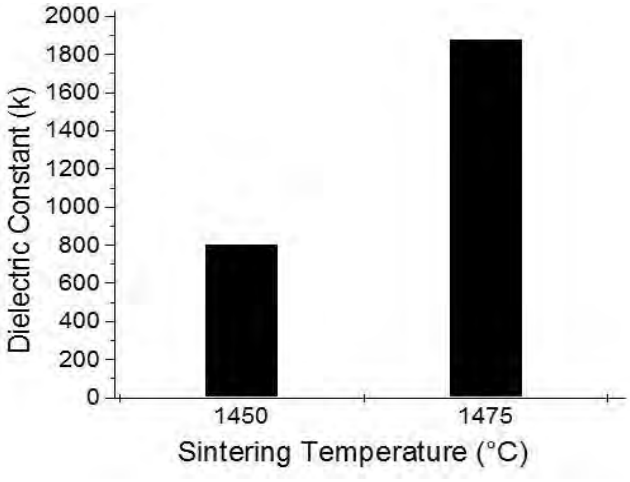

(a)

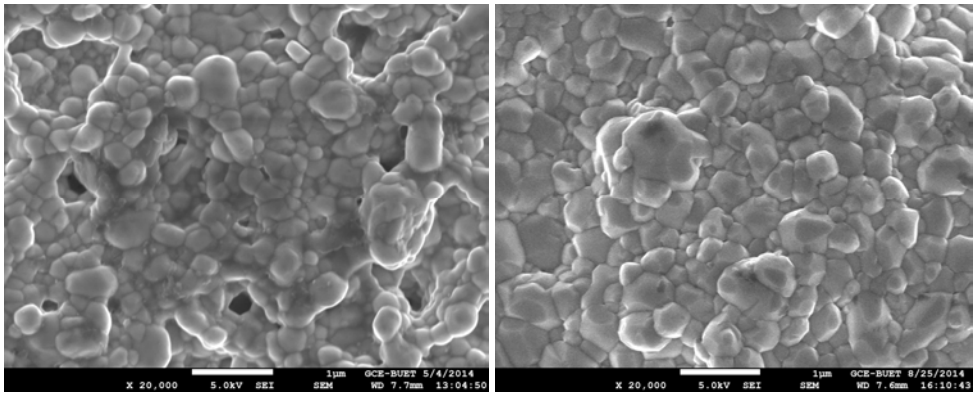

(b) (c)

Figure 4.32 (a) Dielectric Constant Variation Measured at 0.1 kHz of 1.6 mol% Nb Doped Sample being Sintered at Different Sintering Temperatures and their Corresponding Micrographs (b) 1450°C, (c) 1475°C

Figure 4.32 clearly indicates the rise of dielectric constant with sintering temperature. This confirms that 1450°C is not the optimum sintering condition for 1.6 mol% Nb doped $BaTiO_3$ sample. From the micrographs, it is evident that lowering of porosity has been responsible for raising the k values with increasing sintering temperature from 1450°C to 1475°C. However, dielectric constant values are still not satisfactory in using them in capacitors. As already stated, pseudocubic structures may still be persistent in holding down the dielectric constant values [43].

In the light of above context it can be concluded that, Nb provides satisfactory dielectric constant upto the doping level of 0.8 mol% in $BaTiO_3$ being sintered at 1450°C at an applied frequency of 0.1 KHz. However, this temperature is not sufficient for 1.6 mol% Nb doped sample for achieving good density and better dielectric

properties. Moreover, this level of doping has given remarkable grain refining effect as well.

Conclusion

This work was undertaken in order to process and characterize calcined and sintered donor (Nb) doped barium titanate. Following findings have been found through this work.

- Narrow size distribution was obtained for barium carbonate, whereas larger size distributions were found for TiO_2 and Nb_2O_5 which were used as raw materials. This may happen due to different production techniques used for manufacturing different powders.
- 1300°C of calcination temperature produced niobium doped barium titanate which was confirmed by XRD study. XRD patterns not only confirmed successful formation of perovskite structure but also showed formation of secondary phases like $BaNb_{0.5}Ti_{0.5}O_3$ and $Ba_6Ti_{14}Nb_2O_{39}$.
- Loss of tetragonality with Nb addition was confirmed from XRD patterns with the manifestation of lower c/a ratio with increasing doping level. Shrinkage of host lattice due to Nb addition may be responsible for this.
- Bimodal size distribution of particle was observed after calcination for each doping level, and particle size less than 1 micron was produced after calcination, which is a good size for producing fine grain-microstructure necessary for attaining optimum dielectric constant after sintering.
- Slow diffusion and non uniform distribution of Nb into barium titanate were observed in EDX study even after calcination at high temperature for different doping level. This happened because high energy is required to incorporate Nb into $BaTiO_3$.
- Optimum sintering temperature was 1450°C for sample containing 0.4 mol% Nb. Different properties of similar composition were studied, being sintered at different sintering temperatures. Other sintering parameters were optimized by same trial and error method.
- Maximum dielectric constant was 10,000 for the sample containing 0.4 mol% Nb at room temperature. 0.1 KHz or less applied frequency was found appropriate for getting high dielectric constant.
- Lowering of Curie temperature by the addition of Nb was observed. Lower thermal energy requirement for breaking asymmetric balance of Nb-O bond, compared to Ti-O bond, may be responsible for this phenomenon.
- ANOVA modeling identified significant variables such as sintering temperature for density, Nb concentration for grain size and applied frequencies for dielectric constant respectively within specified experimental conditions.

- Refinement of grain size below 700nm, lowering of k values and lowering of density occurred with Nb addition specially for 1.6 mol% Nb. This restricts the doping level for Nb for optimization of dielectric properties of $BaTiO_3$.

Reference

[1] D. Popovici, M. Okuyama and J. Akedo, "*Barium Titanate-Based Materials – a Window of Application Opportunities*", http://www.intechopen.com/books/ ferroelectrics-material-aspects/barium-titanate-based-materials-a-window-of-application-opportunities, Date Accessed: 26-10-2014.

[2] A. J. Moulson and J. M. Herbert, "*Electroceramics"*, John Wiley & Sons Ltd., 2003, pp. 253,340.

[3] "*Ceramic Capacitors"*, http://my.execpc.com/~endlr/ceramic.html, Date Accessed: 26-10-2014.

[4] T. Dechakupt, J. Tangsritrakul , P. Ketsuwan and R. Yimnirun, "*Microstructure and Electrical Properties of Niobium Doped Barium Titanate Ceramics*", Ferroelectrics, 2011, vol. 415, pp. 141–148.

[5] J. F. Becker, "*Capacitors",* http://www.physics.sjsu.edu/becker/physics51 /capacitors. htm, Date Accessed: 26-10-2014.

[6] H. S. Lee, A. S. Lee, K. Y. Baek and S. S. Hwang, "*Low Dielectric Materials for Microelectronics*",http://www.intechopen.com/books/dielectric-material/low-dielectric-materials-for-microelectronics, Date Accessed: 26-10-2014.

[7] C. B. Carter, M. G. Norton, "*Ceramic Materials Science and Engineering"*, Springer, New York, 2007, chapter 7, 24 and 31.

[8] D.W. Richarson, "*Modern Ceramic Engineering-Properties, Processing and Use in Design"*, H C Malone Books, Second Edition Revised and Expanded 1992, pp. 252-254, 260,265.

[9] R. Shaw, "*Ferroelectric Materials*", http://www.doitpoms.ac.uk/tlplib/ferroelectrics /printall.php, Date Accessed: 26-10-2014.

[10] M. M. Vijatović, J. D. Bobić, B. D. Stojanović, *"History and Challenges of Barium Titanate: Part I*", Science of Sintering, 2008, vol. 40, pp. 155-165.

[11] K. Uchino, E. Sadanaga, T. Hirose, "*Dependence of the Crystal Structure on Particle Size in Barium Titanate*", Journal of the Korean Ceramic Society, 1989, vol. 72(8), pp. 1555-1558.

[12] Y. Su, G. J. Weng, "*The Shift of Curie Temperature and Evolution of Ferroelectric Domain in Ferroelectric Crystals*", Journal of the Mechanics and Physics of Solids, 2005, vol. 53, pp. 2071–2099.

[13] T. Ohno, D. Suzuki, H Suzuki, T. Ida, "*Size Effect for Barium Titanate Nano-particles*", KONA Powder and Particle, 2004, vol. 22, pp 195-200.

[14] W. J. Merz, "*The Electric and Optical Behavior of $BaTiO_3$ Single-domain Crystals*", Physical Review, 1949, vol. 76, pp. 1221–1225.

[15] W. J. Merz, "*The Effect of Hydrostatic Pressure on the Curie Point of Barium Titanate Single Crystals*", Physical Review, 1950, vol. 77, pp. 52–54.

[16] W. J. Merz, "*Domain Properties in $BaTiO_3$*", Physical Review, 1952, vol. 88, pp. 421–422.

[17] W. J. Merz, "*Double Hyeteresis Loop of $BaTiO_3$ at the Curie Point*", Physical Review, 1953, vol. 91, pp. 513-517.

[18] W. J. Merz, "*Domain Formation and Domain Wall Motions in Ferroelectric $BaTiO_3$ Single Crystals*", Physical Review, 1954, vol. 95, pp. 690–698.

[19] J. Bera, D. Sarkar, "*Formation of $BaTiO_3$ from Barium Oxalate and TiO_2*", Journal of Electroceramics, 2003, vol. 11(3), pp. 131-137.

[20] U. Manzoor, D .K. Kim, "*Synthesis of Nano-sized Barium Titanate Powder by Solid-state Reaction between Barium Carbonate and Titania*", Journal of Materials Science and Technology, 2007, vol. 23 (5), pp. 655-658.

[21] W. D. Callister Jr., "*Materials Science and Engineering-An Introduction"*, John Wiley & Sons Inc., New York, 2006, pp. 482.

[22] A. Jamal, Md. Naeem, Y. Iqbal, "*Characterization of Barium Titanate Prepared via Mixed Oxide Sintering Route",* Journal of Pakistan Materials Society, 2008, vol. 2(2), pp. 91-95.

[23] T. Bongkarn, N. Phungjit and N. Vittayakorn, "*Effect of Calcination Temperatures on Microstructure and Phase Formation of $Ba(Zr_{0.3}Ti_{0.7})O_3$*", NU Science Journal 2007, vol. 4(S1), pp. 13–21.

[24] B. D. Stojanović, V. R. Mastelaro, C. O. Paiva Santos, J. A.Varela, "*Structure Study of Donor Doped Barium Titanate Prepared from Citrate Solutions*", Science of Sintering, 2004, vol. 36, pp. 179-188.

[25] C. H. Kim, K. J. Park, Y. J. Yoon, Y. T. Kim, and K. H. Hur, "*Formation of Core-Shell Structure in $BaTiO_3$ Grains*", Journal of the Korean Ceramic Society, 2009, vol. 46 (2), pp. 123-130.

[26] Y. J. Kim, J. W. Hyun, H. S. Kim, J. H. Lee, M. Y. Yun, S. J. Noh and Y. H. Ahn, "*Microstructural Characterization and Dielectric Properties of Barium Titanate Solid*

Solutions with Donor Dopants", Bulletin of the Korean Chemical Society, 2009, vol. 30(6), pp 1267-1273.

[27] Y. Yuan , S. R. Zhang, X. H. Zhou, B. Tang, "*Effects of Nb_2O_5 Doping on the Microstructure and the Dielectric Temperature Characteristics of Barium Titanate Ceramics*", Journal of Materials Science, 2009, vol. 44, pp. 3751–3757.

[28] H. I. Hsiang, K. Y. Lin, F. S. Yen, C. Y. Hwang,"*Effects of Particle Size of $BaTiO_3$ Powder on the Dielectric Properties of $BaTiO_3$/Polyvinylidene Fluoride Composites*", Journal of Materials Science, 2001, vol. 36, pp. 3809 – 3815.

[29] C. Miclea, C. Tanasoiu, I. Spanulescu, C. F. Miclea, A. Gheorghiu, L. Amarande, M. Cioangher, C. T. Miclea, "*Microstructure and Properties of Barium Titanate Ceramics Prepared by Mechanochemical Synthesis*", Romanian Journal of Information Science and Technology, 2007, vol. 10(4), pp. 335-345.

[30] C. J. Wang, C. Y. Huang, Y. C. Wu, "*Two-step Sintering of Fine Alumina–zirconia Ceramics*", Ceramics International, 2009, vol. 35(4), pp. 1467-1472.

[31] T. Hoshina, K. Takizawa, J. Li, T. Kasama, H. Kakemoto and T. Tsurumi, "*Domain Size Effect on Dielectric Properties of Barium Titanate Ceramics*", Japanese Journal of Applied Physics, 2008, vol. 47(9), pp. 7607-7611.

[32] M. Kahn, "*Technical Information, Multilayer Ceramic, Capacitor–Materials and Manufacture*", 2004, pp. 2.

[33] B. Carter, "*The Secret to Perfect Terra Sig - A Ball Mill and a little Crocus Martis*", http://carterpottery.blogspot.com/2011/01/secret-to-perfect-terra-sig-ball-mill.html, Date Accessed: 26-10-2014.

[34] S. P. Gupta, "*Advanced Practical Statistics"*, ninth ed., S. Chand & Company, New Delhi, 2002, pp. 759.

[35] K. Kowalski, M. Ijjaali, T. Bak, B. Dupre, J. Nowotny, M. Rekas, C.C. Sorrell, "*Kinetics of Nb Incorporation into Barium Titanate*", Journal of Physics and Chemistry of Solids, 2001, vol. 62, pp. 531-535.

[36] Y. Zhang, J. Hao and J. Qi, "*The Effect of Nb_2O_5 Addition on the Dielectric Properties of $BaTiO_3$-based Ceramics*", Advanced Materials Research, 2011, vol. 287-290, pp. 1108-1111.

[37] B. Cui, P. Yu, J. Tian, H. Guo, Z. Chang, "*Preparation and Characterization of Niobium-Doped Barium Titanate Nanocrystalline Powders and Ceramics*", Materials Science and Engineering A, 2007, vol. 454–455, pp. 667–672.

[38] H. Hughes, D. M. Iddles, I. M. Reaney, "*Niobate-based Microwave Dielectrics Suitable for Third Generation Mobile Phone Base Stations*", Applied Physics Letter, 2001, vol. 79(8), pp. 2952-2954.

[39] A. Goldman, "*Modern Ferrite Technology*", Springer, New York, 2006, pp. 182.

[40] S. Garcia, R. Font, J. Portelles, R. J. Quinones, J. Heiras & J. M. Siqueiros, "*Effect of Nb Doping on (Sr,Ba)TiO_3 (BST) Ceramic Samples*", Journal of Electroceramics, 2001, vol. 6(2), pp. 101–108.

[41] X. Wang, H. L. W. Chan, C. L. Choy, "*Positive Temperature Coefficient of Resistivity Effect in Niobium-doped Barium Titanate Ceramics Obtained at Low Sintering Temperature*", Journal of the European Ceramic Society, 2004, vol. 24, pp. 1227–1231.

[42] N. Maso´, H. Beltra´n, E. Cordoncillo, A. Arenas Flores, P. Escribano, D. C. Sinclair and A. R. West, "*Synthesis and Electrical Properties of Nb-doped $BaTiO_3$*", Journal of Materials Chemistry", 2006, vol. 16, pp. 3114–3119.

[43] B. D. Stojanovic, C. R. Foschini, M. A. Zaghete, F. O. S. Veira, K. A. Peron, M. Cilense, J. A. Varela, "*Size Effect on Structure and Dielectric Properties of Nb-doped Barium Titanate*", Journal of Materials Processing Technology, 2003, vol. 143–144, pp. 802–806.